Seismic detection of the untransformed 'basaltic' oceanic crust subducting into the mantle

Sadaki Hori *National Research Center for Disaster Prevention, Tennodai 3–1, Sakura-mura, Niihari-gun, Ibaraki-ken 305, Japan*

Hiroshi Inoue and Yoshio Fukao *Department of Earth Sciences, Nagoya University, Chikusa, Nagoya 464, Japan*

Motoo Ukawa *National Research Center for Disaster Prevention, Tennodai 3–1, Sakura-mura, Niihari-gun, Ibaraki-ken 305, Japan*

Summary. Subcrustal earthquakes occur in a slab-like zone beneath SW Japan in association with the subduction of the Philippine Sea plate. They generate a distinct pair of P and S later phases with anomalously low apparent velocities of about 7 and $4 \, \mathrm{km \, s^{-1}}$, which cannot be explained by a laterally homogeneous velocity structure. These later phases are observed for particular source–receiver geometries: the sources at depths shallower than 50–60 km and the receivers beneath which the subcrustal seismic zone comes in contact with the bottom of the continental crust. We examined the nature of these later phases using two methods. One is to determine two types of apparent velocities, an 'event-common' apparent velocity and a 'station-common' apparent velocity, which may be different from one another for a laterally inhomogeneous velocity structure. The other is to trace seismic rays numerically for a laterally heterogeneous velocity model. An extensive analysis using these two methods leads to a conclusion that the slab-like seismic zone constitutes a low-velocity channel in the uppermost mantle with P and S velocities comparable to those of the lower continental crust beneath SW Japan. The waves trapped within the low-velocity channel escape from it through its contact with the continental Moho and are observed as a distinct pair of later phases. The head waves guided by the bottom boundary of the low-velocity channel are observed as weak arrivals of initial phases. The thickness (<10 km) and the velocities ($V_P \approx 7 \, \mathrm{km \, s^{-1}}$, $V_S \approx 4 \, \mathrm{km \, s^{-1}}$) of the subcrustal seismic zone indicates that it is made up of the 'untransformed basaltic oceanic crust' subducted with the underlying lithospheric mantle and that the transformation of basalt to eclogite does not take place in the subducting slab at least down to depths of 50–60 km. We present laterally heterogeneous structural models of the crust and the

uppermost mantle along two profiles in SW Japan. The models are characterized by an apparent thickening of the lower continental crust in particular regions due to a direct contact of the subducting oceanic crust to the continental Moho. Such features are qualitatively consistent with the results of explosion seismology and with the Bouguer anomaly pattern in the relevant regions. The oceanic lithosphere with the untransformed 'light' oceanic crust at its top might still be buoyant after subduction, a factor which must be taken into account in considering the driving mechanisms of plate tectonics, the slab geometry and the earthquake-related tectonic process.

1 Introduction

Most of the oceanic crust is considered to subduct into the mantle at the trench as a part of the oceanic lithosphere (Ringwood 1975). The main layer of the oceanic crust is traditionally believed to be of basaltic or gabbroic composition (Yorder & Tilley 1962; Christensen & Salisbury 1975), a picture now basically supported by several lines of evidence, such as seafloor dredging, drilling (e.g. Engel & Engel 1964; Kay, Hubbard & Gast 1970) and oceanic refraction studies (e.g. McConnell, Gupta & Wilson 1966; Shor *et al.* 1968). Experimentally basalt or gabbro transforms to eclogite at high pressure (Ringwood & Green 1966; Cohen, Ito & Kennedy 1967; Green & Ringwood 1972). We therefore expect this transformation to take place upon subduction of the oceanic crust. The basalt–eclogite transformation is important in many aspects such as the driving mechanisms of lithospheric plates (Ringwood 1972, 1976), the thermal regime of island arcs (Delany & Helgeson 1978) and the earthquake-related tectonic process (Ruff & Kanamori 1983). This transformation is, however, affected by many factors including temperature (Ito & Kennedy 1971; Wyllie 1982), water content (Ahrens & Schubert 1975), bulk rock chemical composition (Ringwood 1974) and, perhaps, stress environment. Since it is practically impossible to evaluate all these factors correctly, it would not be feasible to estimate the accurate depth of the transformation by a petrological approach.

Seismic observation is an alternative approach toward this problem. As is generally known, seismic velocities of basaltic rocks are substantially lower than those of mantle rocks including eclogitic rocks (Christensen 1972; Manghani, Ramananantoandro & Clark 1974). Therefore a low-velocity zone dipping from the trench towards inland might be observed if the oceanic crust penetrating into the mantle remains basaltic. Once such a low-velocity zone were identified, its leading edge might indicate the basalt–eclogite transition depth. In fact, it has been suggested that a low-velocity zone exists in the vicinity of the deep seismic zone from phase-conversion analyses of body waves (Okada 1979; Nakanishi 1980). However, it is still open to discussion whether or not the low-velocity zone can be interpreted as the subducted oceanic crust (Langston 1981; Nakanishi, Suyehiro & Yokota 1981). Okada (1979), for example, considered the low-velocity zone to be a zone of partial melting due to frictional heating accompanied with the descending motion of the slab. Explosion seismology to date has not yet detected such a low-velocity layer because, perhaps, the low-velocity layer is, if anything, too thin and too deep to be detected.

We report in this paper extraordinary seismic waves emergent from the untransformed oceanic crust dipping into the mantle. The preliminary results of our study have been reported by Fukao, Hori & Ukawa (1983), which is hereafter referred to as paper I. In this paper we examine these waves in more detail with the additional data using a 2-D ray tracing technique. The ray tracing technique is shown to be a powerful tool in examining a highly complicated velocity structure.

2 Seismicity and earthquake data

South-west Japan is characterized by the subduction of the Philippine Sea plate against the Eurasian plate along the Nankai–Suruga trough (Fitch & Scholz 1971; Kanamori 1972b; Ando 1975). Yet we observe neither deep seismic activities nor distinct volcanic activities associated with this subduction. This feature might be related to the fact that the plate convergence in this region is supposed to have started only several million years ago (Kanamori 1972b; Seno 1977).

There is, however, a prominent seismic activity in the vicinity of the Moho. The seismic zone is slab-like and dipping landwards at low angles (10–30°). These earthquakes are believed to be caused by the subducting motion of the Philippine Sea plate (Kanamori 1972a; Shiono 1977; Hashimoto 1982; Ukawa 1982) so that they delineate the configuration of the downgoing slab of lithospheric plate (Mizoue 1977; Aoki 1980). We call these earthquakes 'subcrustal earthquakes' regardless of whether their foci are above or below the Moho.

Recent microearthquake observations revealed that the thickness of the subcrustal seismic zone is less than 10 km (e.g. Ukawa 1982). The shape of this seismic zone is depicted in Fig. 1 by focal depth contours based on Aoki (1980) and Mizoue *et al.* (1983). Two active regions are enclosed by solid lines, one beneath the southern part of the Chubu district (region A) and the other beneath the Kii peninsula (region B). The seismic zone concaves downward in each region and reaches a depth of 60 km beneath the central Chubu and a depth of 80 km beneath the NW of the Kii peninsula. The seismic activity further downward and landward becomes quite sparse as if the seismic zone is truncated.

The Moho lies at a depth of 30–33 km in both regions A and B (Mizoue 1971; Aoki *et al.* 1972; Ikami 1978), a feature supported by surface wave analyses (Aki 1961; Kaminuma 1966a, b) and by gravity analyses (Kanamori 1963a, b; Mikumo 1966). A large part of the subcrustal seismic zone, therefore lies below the Moho and its upward and seaward continuation seems to come in direct contact with the Moho in the coastal region. Because of its lateral warping the seismic zone beneath the Chubu district (region A) seems to contact with the Moho at its western end in a narrow zone extending north-westward from Ise Bay to Lake Biwa (see Fig. 1). It is uncertain how this seismic zone connects to that in the Kinki district (region B) because of the sparse seismicity.

In the present study we investigate 20 subcrustal earthquakes occurring beneath region A from 1978 to 1981 and 32 subcrustal earthquakes occurring beneath region B from 1980 to 1984. We use hypocentral data given by the Regional Center for Earthquake Prediction Observation (RCEPO) of Nagoya University and the Wakayama Microearthquake Observatory (WMO) of the University of Tokyo. They are listed in Table 1. Epicentres of the earthquakes are also plotted in Fig. 1. Note that the hypocentral parameters used in paper I were provided by the Japan Meteorological Agency (JMA) whose network is less dense than those of the above organizations. We analyse three-component seismograms telemetered to the Abuyama Seismological Observatory (ASO) of Kyoto University, the National Research Center for Disaster Prevention (NRCDP) and RCEPO.

3 Anomalous later phase

At some stations we observe a distinct pair of later phases after the initial P and S arrivals from the subcrustal earthquakes described above. Fig. 2 shows an example of three-component seismograms exhibiting such later phases. The later phase after the initial P is predominant in the vertical component and the later phase after the initial S is predominant in the horizontal components. Hence the phases are interpreted as the compressional and the

172   S. *Hori* et al.

Table 1. (a) List of earthquakes, region A.

No.	Origin time (GMT)						Hypocentre						Depth	M
							Longitude			Latitude				
	y	m	d	h	m	s	d	m	s	d	m	s	km	
A01	1978	04	03	18	48	26.82	137	26	00	35	19	18	46.8	3.5
A02	1980	04	01	16	40	08.28	137	13	48	35	24	00	49.2	2.8
A03	1980	04	09	07	12	58.61	137	25	24	35	00	00	34.5	2.6
A04	1980	04	30	19	06	19.86	137	25	36	35	57	48	35.1	3.1
A05	1980	06	04	22	02	48.64	137	24	48	35	19	00	42.5	2.6
A06	1980	06	21	03	10	49.96	137	14	24	35	14	42	38.7	2.8
A07	1980	08	28	01	31	18.80	137	19	54	35	17	54	44.9	2.6
A08	1980	09	01	12	48	50.97	137	32	12	35	10	30	40.9	3.6
A09	1980	10	13	18	45	10.72	137	14	54	35	13	06	40.6	2.8
A10	1981	03	19	10	34	46.07	137	15	36	35	19	54	45.9	2.7
A11	1981	04	27	16	46	59.22	136	54	48	34	53	24	35.4	3.2
A12	1981	05	02	03	42	59.17	137	00	24	35	14	48	41.3	3.3
A13	1981	05	06	10	12	00.82	137	09	54	34	58	24	34.0	2.5
A14	1981	05	11	00	40	38.18	137	33	18	35	11	18	40.2	2.5
A15	1981	05	14	14	00	10.19	137	01	30	35	14	12	36.3	2.6
A16	1981	05	28	23	23	22.92	137	18	42	35	05	36	31.2	3.2
A17	1981	06	15	04	34	48.68	136	53	48	35	25	42	38.1	3.1
A18	1981	07	26	23	46	46.84	137	28	36	34	56	24	31.3	2.9
A19	1981	08	18	14	08	41.48	137	38	30	35	20	06	44.3	5.1
A20	1981	08	28	16	05	00.78	136	57	42	35	22	24	42.1	3.2

(b) List of earthquakes, region B.

No.	Origin time (GMT)						Hypocentre						Depth	M
							Longitude			Latitude				
	y	m	d	h	m	s	d	m	s	d	m	s	km	
B01	1980	10	22	19	30	04.01	135	08	42	33	42	35	33.4	2.7
B02	1980	12	25	04	12	37.61	135	31	53	33	54	25	46.8	3.0
B03	1980	12	28	14	55	00.70	134	58	06	33	41	28	34.8	3.3
B04	1981	03	05	23	28	23.80	135	26	55	33	50	56	40.5	4.2
B05	1981	09	02	11	57	08.71	135	35	29	33	52	01	38.0	3.3
B06	1981	10	06	05	44	05.66	135	25	43	34	25	31	81.4	3.8
B07	1981	10	27	08	06	09.80	135	54	31	34	08	41	57.0	2.9
B08	1981	11	12	17	30	54.75	135	17	43	33	49	10	45.7	3.3
B09	1981	11	14	20	29	49.78	135	01	05	33	38	26	33.7	3.7
B10	1982	01	14	14	24	32.73	135	17	05	33	43	39	38.3	2.9
B11	1982	02	11	15	43	36.84	135	50	08	34	00	30	41.2	3.2
B12	1982	03	03	01	14	54.83	135	35	19	33	53	59	51.4	2.8
B13	1982	05	07	20	36	22.34	135	28	44	33	54	35	53.3	3.7
B14	1982	05	26	05	25	59.60	135	39	59	34	13	08	58.1	3.3
B15	1982	06	21	15	57	03.80	135	27	56	33	53	29	54.2	5.0
B16	1982	08	18	11	08	19.09	135	53	19	33	51	01	48.8	3.6
B17	1982	09	20	08	42	59.89	135	35	49	34	00	54	52.1	2.5
B18	1982	10	09	02	43	43.34	136	01	34	34	34	45	61.7	3.9
B19	1982	10	19	18	22	44.29	135	24	44	33	52	33	51.5	2.9
B20	1983	01	07	12	43	41.44	136	20	23	34	23	26	34.6	2.5
B21	1983	03	17	17	32	14.48	136	24	19	34	37	29	36.2	2.5
B22	1983	04	10	18	49	43.42	136	54	26	34	28	28	31.1	2.5
B23	1983	05	08	08	49	24.14	135	27	22	33	50	48	43.9	3.6
B24	1983	07	13	04	41	49.52	135	22	00	33	51	38	52.2	4.0
B25	1983	07	18	00	20	49.50	135	45	21	34	14	29	59.1	4.6
B26	1983	09	08	13	03	40.30	135	29	14	34	10	44	63.0	4.0
B27	1983	09	11	04	48	11.53	136	37	56	34	34	20	34.6	3.0
B28	1983	10	30	09	25	48.16	136	26	38	34	32	52	34.9	2.6
B29	1983	11	02	13	35	43.62	135	31	12	33	57	39	48.7	3.6
B30	1983	12	18	10	20	42.20	135	23	21	33	49	37	49.9	3.3
B31	1984	02	10	19	49	25.06	135	42	04	34	04	02	55.2	5.5
B32	1984	03	11	07	53	56.52	135	19	33	33	48	39	47.8	3.3

shear waves respectively. Figs 3 and 4 show the seismograms pasted up in the order of epicentral distances. The arrivals of the initial and the later phases are indicated by solid lines to which the values of their apparent velocities are attached. The initial *P*- and *S*-waves are in general very weak. By contrast the later phases are clearly and systematically seen with large amplitues. They seem to contain several wavelets which tend to be dispersed at distant stations.
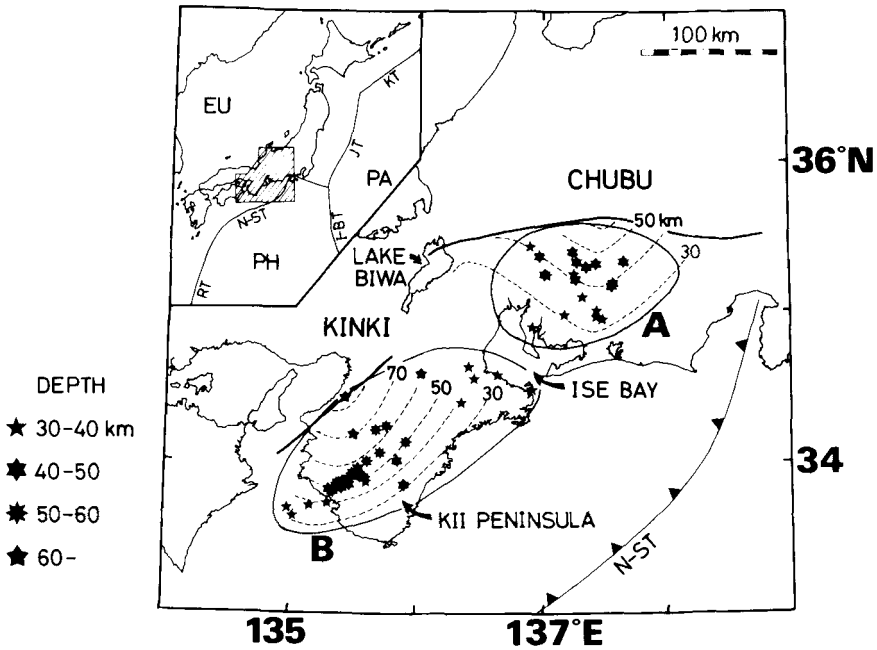
Figure 1. Epicentral distribution of subcrustal earthquakes listed in Table 1. Symbols are classified by the focal depths. Two active regions (A and B, see text) are enclosed by solid curves. Thick solid lines and broken lines indicate the leading edge and the depth contours of the top of the seismic zones respectively. The lithospheric plates and their convergent boundaries around Japan are also shown in the left top. EU: Eurasian plate, PA: Pacific plate, PH: Philippine Sea plate, KT: Kurile trench, JT: Japan trench, I-BT: Izu–Bonin trench, N–ST: Nankai–Suruga trough, RT: Ryukyu trench.
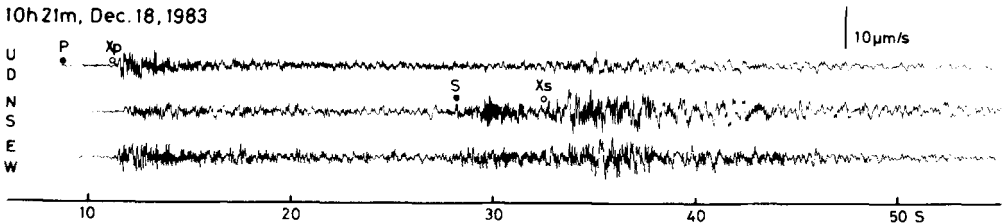
Figure 2. Three-component seismograms exhibiting distinct later phases for event B30 (Table 1) recorded at a coastal station (ABN, Akabane) in the Chubu district. Initial and later arrivals are indicated by filled and open circles and denoted by P or S and Xp or Xs respectively.

These later phases are always seen for subcrustal earthquakes shallower than 50–60 km and for two source–receiver geometries such as:

case A: events beneath region A observed at the inland stations of the Kinki district.
case B: events beneath region B observed at the coastal stations of the Chubu district.

Fig. 5 shows these two cases, where the corresponding paths are indicatd by solid arrows. Dotted arrows are, on the other hand, the paths for which we never observe the distinct later phases. Two such paths are from events beneath region A to the inland stations of the Chubu district and from events beneath region B to the inland stations of the Kinki district. Examples of the seismograms for such paths are shown in Fig. 6 where the initial phases are very clear
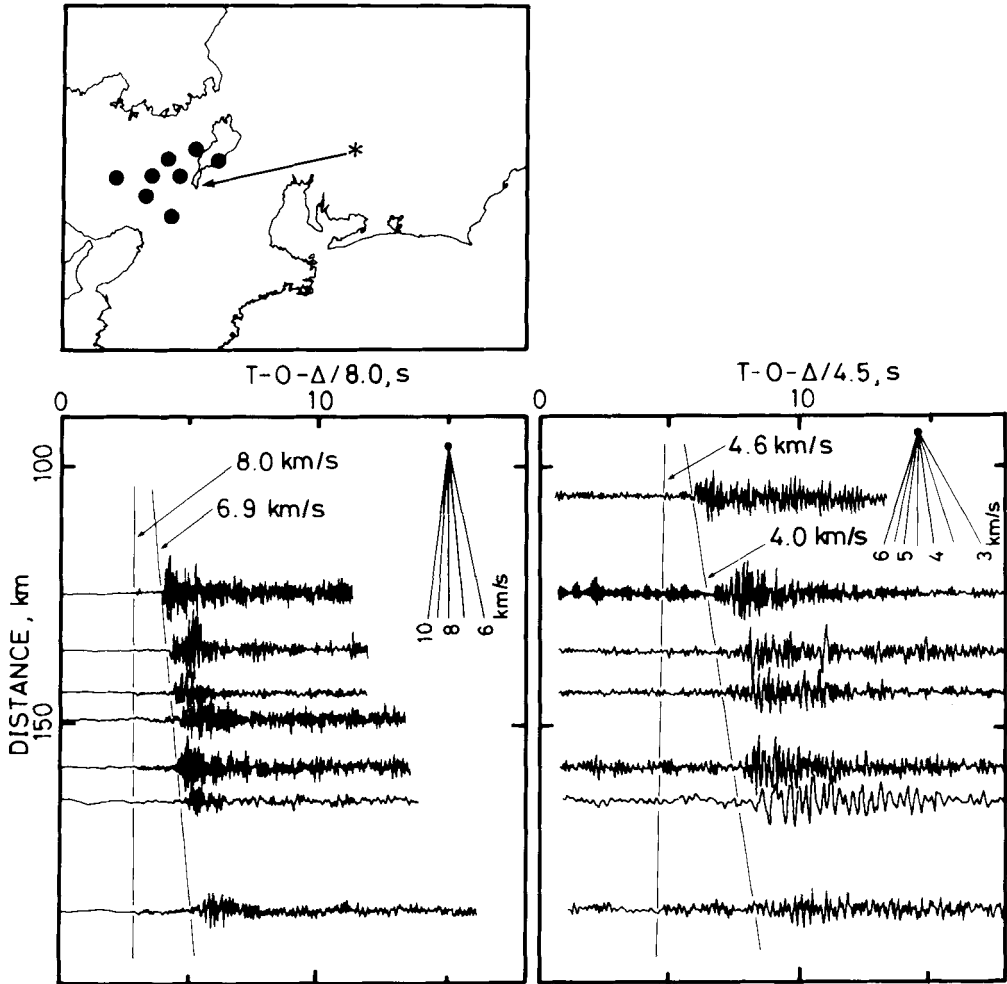
Figure 3. Seismograms of *P* (left) and *S* (right) waves for event A09 (Table 1) recorded at inland stations in the Kinki district. Reduction velocities are 8.0 and 4.5 km s⁻¹ for *P*- and *S*-waves. Initial and later arrivals are indicated by solid lines to which the values of their apparent velocities are attached. Locations of the epicentre and stations are shown at the top.

and not followed by any prominent later phases. As shown in Fig. 5, the seismic zone becomes progressively shallower along the paths indicated by the solid arrows whereas it becomes deeper and eventually truncated along the paths indicated by the dotted arrows.

Some subcrustal earthquakes occur at depths greater than 50–60 km beneath the Kii peninsula. The later phases are not observed for such deeper events even at the same stations as in case B. Fig. 7 shows an example of seismograms for such an event, which shows the initial phases of large amplitudes with clear onsets followed by no such systematic later phases, as seen in Fig. 3. This difference in waveform seems to be associated with the difference in focal depth. To get a detailed picture we classified 52 subcrustal earthquakes listed in Table 1 into two types in terms of their waveforms. If such distinct later phases as shown in Fig. 2 are observed, the earthquake is categorized as type I. If not, the earthquake is categorized as type II. Fig. 8 shows the result of this classification. The later phases are
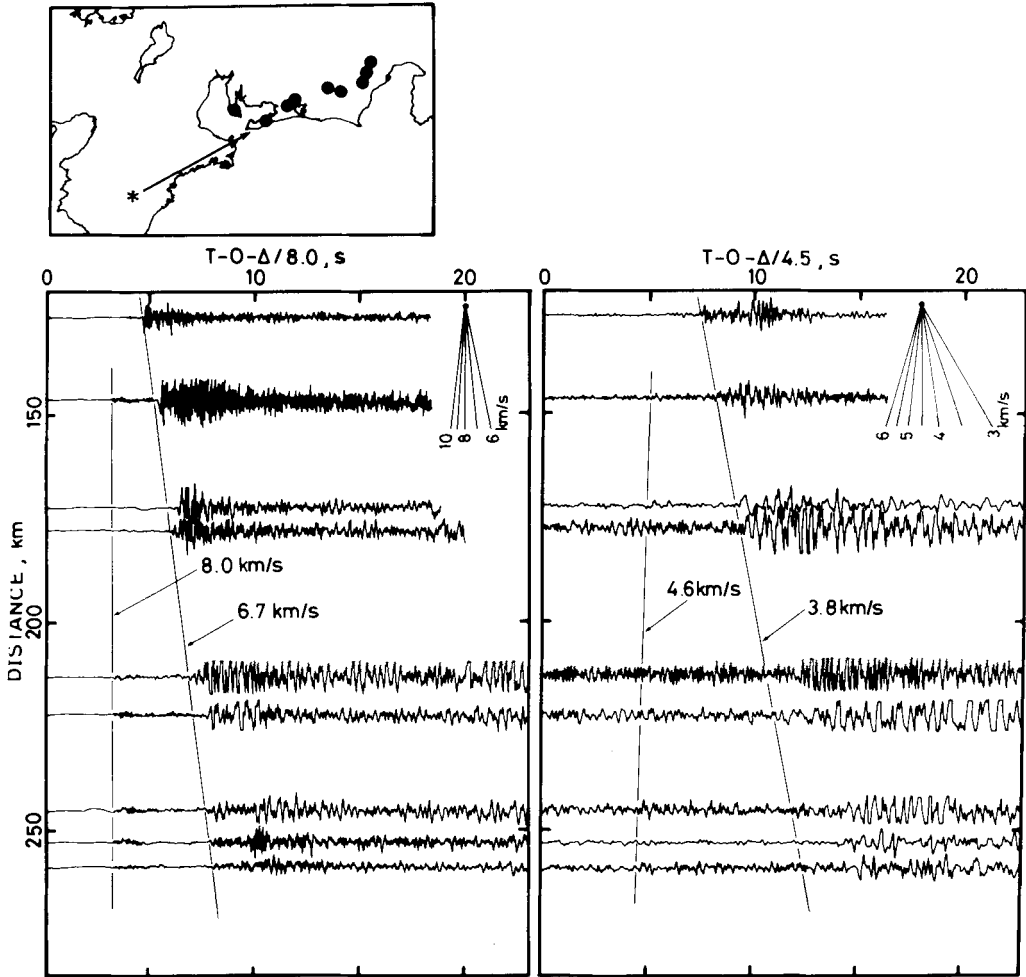
Figure 4. Seismograms for event B11 (Table 1) recorded at coastal stations in the Chubu district. See Fig. 3 for the details.

consistently observed for earthquakes shallower than 50 km. On the other hand, they are never seen for earthquakes deeper than 60 km. The transition from type I to type II occurs in a depth range of 50–60 km.

Table 2 summarizes the observed apparent velocities of the initial and the later phases and their averages. The apparent velocities for each event were obtained by least squares fitting to the arrival-time data directly read from the records. They seem to contain quite large errors because of the ambiguity of the onsets, particularly for the cases of the initial phases. To obtain the average apparent velocities we weighted more heavily the data with a larger number of observations and a larger span of observational stations. Practically we used rather arbitrarily a weight proportional to the number of observations and the rms of the residuals of epicentral distances from their mean. For the average apparent P and S velocities of the initial phases we obtained a value of about $8.1 \, \text{km s}^{-1}$ and a value of 4.6–$4.7 \, \text{km s}^{-1}$ respectively in both cases A and B. These values are somewhat higher than the uppermost mantle P and S velocities in the relevant regions which are 7.8–7.9 and 4.4–$4.5 \, \text{km s}^{-1}$ respectively (Kanamori
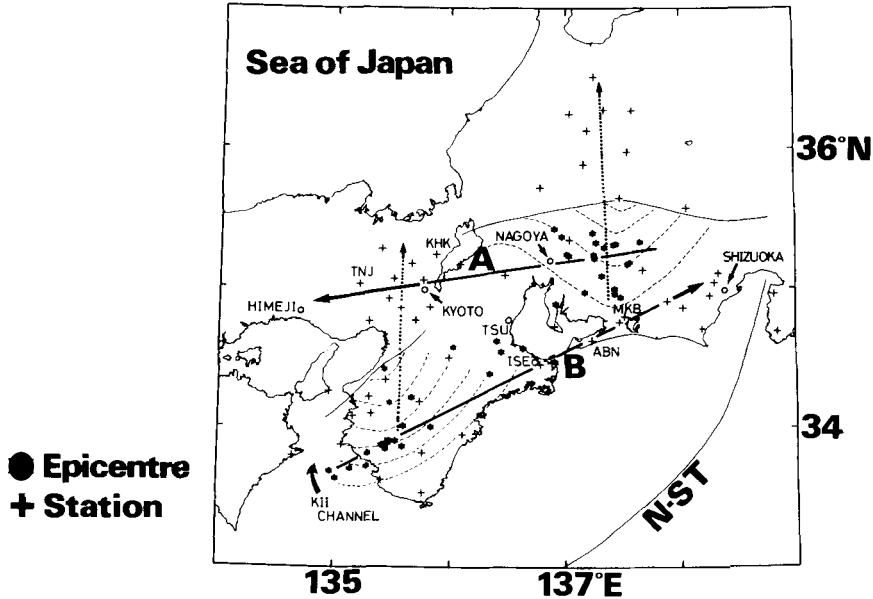
Figure 5. Source–receiver geometries and the corresponding ray paths. Epicentres and seismic stations are indicated by asterisks and crosses respectively. Solid arrows indicate the paths for which the later phases are clearly seen (A and B represent cases A and B, see text). For the paths indicated by the dotted arrows, no systematic later phases are observed. Seismic stations TNJ, KHK, ABN and MKB appear in Fig. 12.

& Tsumura 1971; Ukawa & Fukao 1982). The apparent P and S velocities of the later phases were determined to be less than 7 and less than $4 \, \mathrm{km \, s}^{-1}$ respectively. These apparent velocities are substantially lower than the mantle velocities and rather comparable to the velocities of the lower continental crust and to the velocities of the main layer of the oceanic crust. In view of the consistent appearance of both the P and S later phases, these phases are considered to be of the same origin. Their apparent velocities are, however, too low to invoke a laterally homogeneous velocity structure for which the apparent velocities for any phases must be higher than the P and S velocities at the focus.

One might consider the P later phase as an Sp-wave, the P-wave converted from the S at the Moho discontinuity (Ito 1977). Its ray path toward distant receivers becomes nearly horizontal in the lower crust so that the apparent velocity is expected to agree with the P velocity of the lower crust. Arrival times of such Sp-waves, however, must be sensitive to a focal depth change because they travel below the Moho obliquely at the shear-wave velocity. For example, two events at depths of 35 and 50 km would show a time difference of about 3 s at large distances. To examine whether this is the case or not, we plot the travel times of the initial and later phases against distance for case A in Fig. 9. The symbols are classified by the focal depths. In this figure, no systematic dependence of the arrival times on the focal depths is recognized, indicating that the Sp-wave is not the adequate explanation for the P later phase. Moreover, this explanation cannot account for the presence of the S later phase consistent with the P later phase. To explain both the P and S later phases, it is necessary to consider a laterally heterogeneous velocity structure that permits some 'anomalous' propagation path.

For type II events we obtained very high apparent velocities for both P and S initial arrivals (Table 2). This is, however, a spurious result of including the data at short distances. As can

be seen in Fig. 7, the *P* and *S* arrival-time curves show an inflection in a distance range between 100 and 150 km for type II events. If the data at such distances are discarded, we obtain the apparent velocities similar to those for type I events.

4 Origin of the later phases

In paper I we heuristically derived a structural model that explains the observation. We now discuss the model in a more quantitative way, using the method of seismic ray tracing. The computer program for 2-D ray tracing was written by the authors for the analysis of explosion seismic data (Inoue & Fukao 1984). The algorithm is summarized as follows.
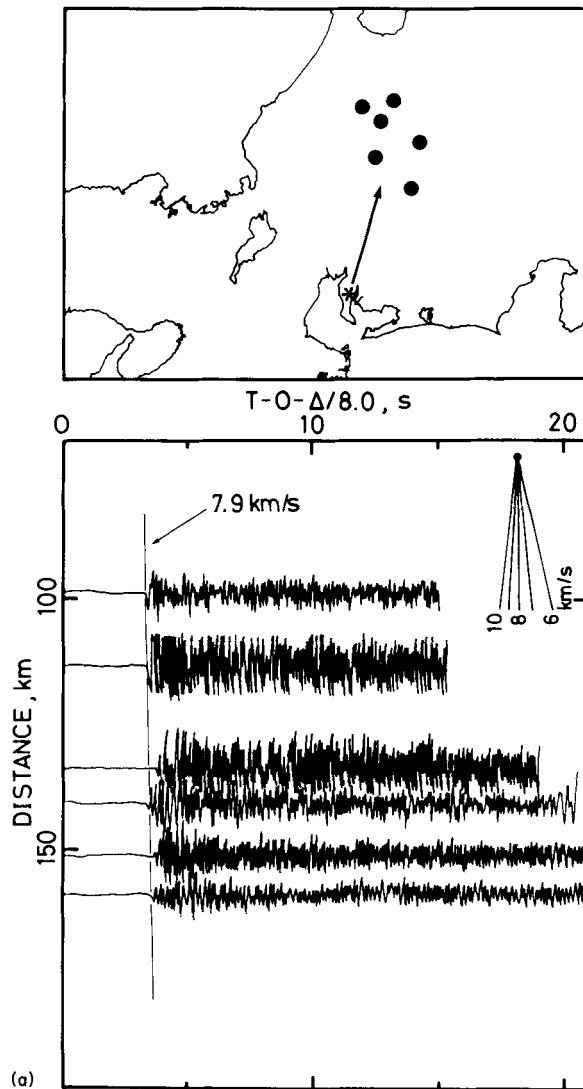
Figure 6. (a) Seismograms of *P*-waves for event A11 (Table 1) recorded at inland stations in the Chubu district. (b) Seismograms of *P*-waves for event B08 (Table 1) recorded at inland stations in the Kinki district. Amplitudes abruptly diminish a few seconds after the initial arrivals because of auto-gain controlling.
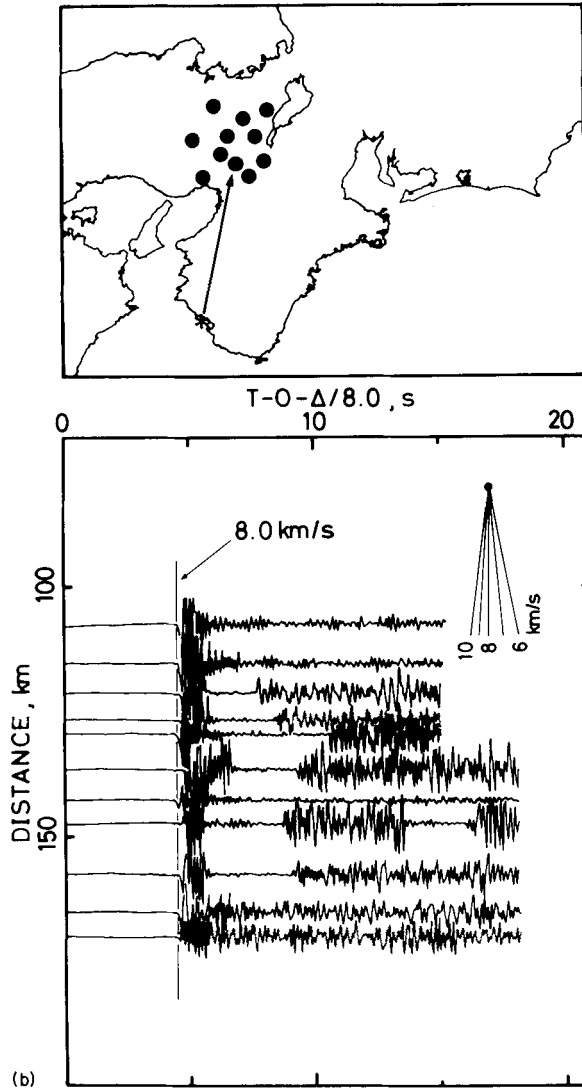
Figure 6 – *continued*

The model consists of 2-D inhomogeneous media having no discontinuities. A discontinuity is replaced by a thin transition zone, so that all kinds of waves due to the discontinuity such as subcritical reflections, *P* to *S* or *S* to *P* conversions, surface waves and headwaves are not included. A superposition of hyperbolic tangent is used for the velocity distribution function, which is the same type of expression as used by Gebrande (1976). Ray paths (x, z) and travel times (t) for a certain emergent angle at the source are calculated to solve an initial value problem of the ray equations:

$$dx/dt = v \sin i,$$

$$dz/dt = v \cos i,$$

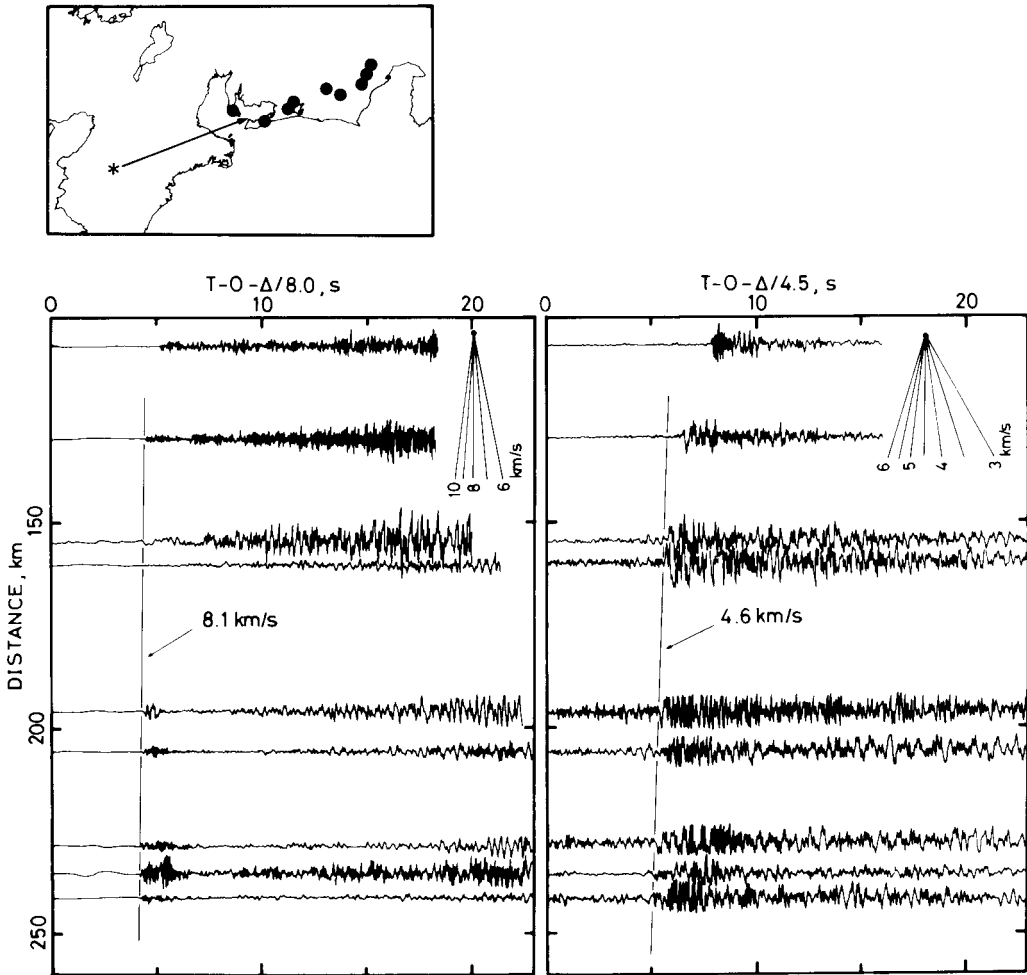$$di/dt = \partial v/\partial z \sin i - \partial v/\partial x \cos i,$$

Figure 7. Seismograms of *P*- and *S*-waves for event B07 (Table 1) recorded at coastal stations in the Chubu district. Waveforms are quite different from those in Fig. 3 in spite of a similar source–receiver geometry.
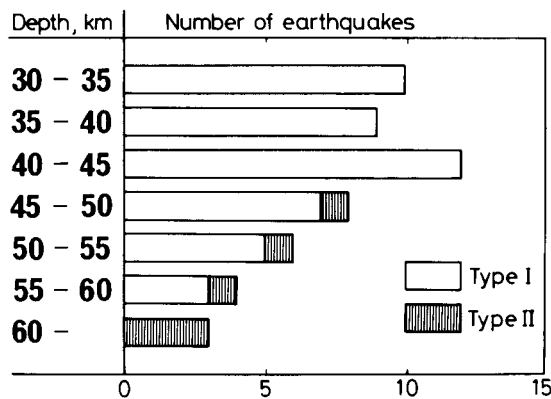

Figure 8. Classification of the subcrustal earthquakes listed in Table 1. Type I: earthquakes exhibiting distinct later phases with apparent velocities significantly lower than the velocities of the uppermost mantle: Type II: earthquakes exhibiting clear initial phases followed by no systematic later phases.

Table 2. (a) Apparent velocities, region A.

No.	Type	V1 km/s	N1	V2 km/s	N2	V3 km/s	N3	V4 km/s	N4
A01	I	7.86±0.14	8	6.74±0.10	8	4.61±0.05	8	3.94±0.17	8
A02	I	7.89±0.14	8	6.59±0.30	8	4.52±0.05	6	3.75±0.08	5
A03	I	–	1	6.78±0.27	7	5.66±0.10	4	3.96±0.06	7
A04	I	7.91±0.08	8	7.02±0.18	8	4.77±0.17	6	3.85±0.03	8
A05	I	7.91±0.29	4	6.78±0.14	7	4.86±0.03	6	4.02±0.04	6
A06	I	8.40±0.36	6	6.73±0.12	7	4.42±0.07	6	3.89±0.05	7
A07	I	8.22±0.18	6	7.00±0.28	7	4.83±0.08	7	3.94±0.04	7
A08	I	8.68±0.11	7	7.00±0.15	7	4.70±0.04	6	3.92±0.05	7
A09	I	7.99±0.07	7	6.81±0.09	7	4.54±0.08	6	3.97±0.05	7
A10	I	8.19±0.32	6	6.89±0.12	7	4.63±0.09	7	4.09±0.03	7
A11	I	–	0	7.42±0.05	9	–	0	3.94±0.08	8
A12	I	7.93±0.04	7	7.26±0.22	7	4.56±0.01	6	3.93±0.06	7
A13	I	8.24±0.10	7	7.20±0.15	7	5.23±0.00	2	4.10±0.06	7
A14	I	8.45±0.16	6	7.12±0.21	6	4.67±0.05	5	4.06±0.04	7
A15	I	8.21±0.20	5	7.13±0.07	5	4.41±0.03	5	3.98±0.05	5
A16	I	7.97±0.19	5	6.87±0.07	5	4.33±0.05	5	3.92±0.04	5
A17	I	8.19±0.09	7	7.00±0.10	7	4.53±0.11	5	3.89±0.08	6
A18	I	7.57±0.28	3	7.08±0.09	9	4.41±0.00	2	3.99±0.07	8
A19	I	8.00±0.06	11	6.87±0.21	9	–	0	–	0
A20	I	8.03±0.06	7	6.95±0.06	7	4.58±0.08	7	3.85±0.06	8
AVRG		8.09±0.22		6.96±0.19		4.60±0.15		3.95±0.08	

V1, V2, V3, V4: apparent velocities and their standard deviations of the initial P, the later P, the initial S and the later S phases.

N1, N2, N3, N4: number of arrival time data used in the calculation.

AVRG: weighted mean and ± weighted rms of residuals of apparent velocity. Weights are proportional to the number of observations and the rms of residuals of epicentral distances form their mean.

(b) Apparent velocities, region B.

| No.	Type	V1 km/s	N1	V2 km/s	N2	V3 km/s	N3	V4 km/s	N4
B01	I	–	0	6.52±0.21	3	–	0	3.51±0.05	3
B02	I	–	1	7.31±0.03	3	4.24±0.00	2	3.84±0.16	3
B03	I	7.63±0.10	5	6.42±0.08	6	±	0	3.70±0.11	6
B04	I	8.78±1.16	4	6.60±0.09	6	–	0	3.69±0.16	4
B05	I	7.29±0.91	3	6.58±0.07	9	–	0	3.75±0.07	9
B08	I	–	1	6.47±0.14	8	4.66±0.07	7	3.87±0.09	8
B09	I	–	0	6.42±0.16	8	–	0	3.50±0.11	6
B10	I	–	1	6.15±0.15	8	–	0	3.37±0.05	5
B11	I	8.47±0.00	2	6.55±0.09	9	–	0	3.56±0.08	9
B13	I	8.46±0.09	6	6.43±0.18	6	4.72±0.14	4	4.06±0.04	3
B14	I	–	0	6.40±0.15	7	–	0	3.78±0.08	8
B15	I	8.30±0.12	8	6.45±0.29	5	5.01±0.13	4	3.65±0.23	3
B17	I	–	1	6.22±0.10	7	–	1	3.64±0.03	7
B19	I	8.41±0.00	2	6.30±0.18	4	–	1	3.58±0.10	7
B20	I	9.33±0.00	2	6.21±0.00	2	4.94±0.00	2	4.00±0.15	3
B21	I	7.25±0.27	3	6.73±0.29	6	4.71±0.00	2	3.75±0.11	5
B22	I	7.99±0.19	3	7.60±0.28	3	4.28±0.10	3	3.35±0.07	3
B23	I	8.21±0.15	8	6.53±0.11	8	4.53±0.00	2	3.63±0.09	8
B24	I	8.11±0.09	7	6.39±0.08	9	4.82±0.05	8	3.82±0.15	8
B25	I	8.31±0.10	8	6.98±0.11	7	4.56±0.08	4	3.79±0.02	4
B27	I	7.42±0.25	6	6.70±0.09	6	4.71±0.41	3	3.34±0.07	4
B28	I	7.25±0.21	4	6.83±0.40	4	–	1	3.88±0.09	7
B29	I	8.13±0.11	6	6.44±0.06	8	4.65±0.14	7	3.75±0.05	8
B30	I	8.36±0.12	8	6.48±0.08	9	4.45±0.08	7	3.69±0.10	8
B31	I	8.63±0.05	8	6.66±0.07	5	–	1	–	0
B32	I	7.84±0.15	5	6.36±0.13	6	–	0	3.45±0.10	3
AVRG		8.09±0.42		6.51±0.21		4.65±0.19		3.68±0.14	
B06	II	8.82±0.21	9	–		5.12±0.08	9	–	
B07	II	8.60±0.21	9	–		5.01±0.16	9	–	
B12	II	8.40±0.13	9	–		6.50±0.32	7	–	
B16	II	8.00±0.10	5	–		4.66±0.03	5	–	
B18	II	8.58±0.19	6	–		–	0	–	
B26	II	10.92±1.48	3	–		4.94±0.00	2	–	
AVRG		8.69±0.57		–		5.28±0.53		–	

Explanations are the same as (a).
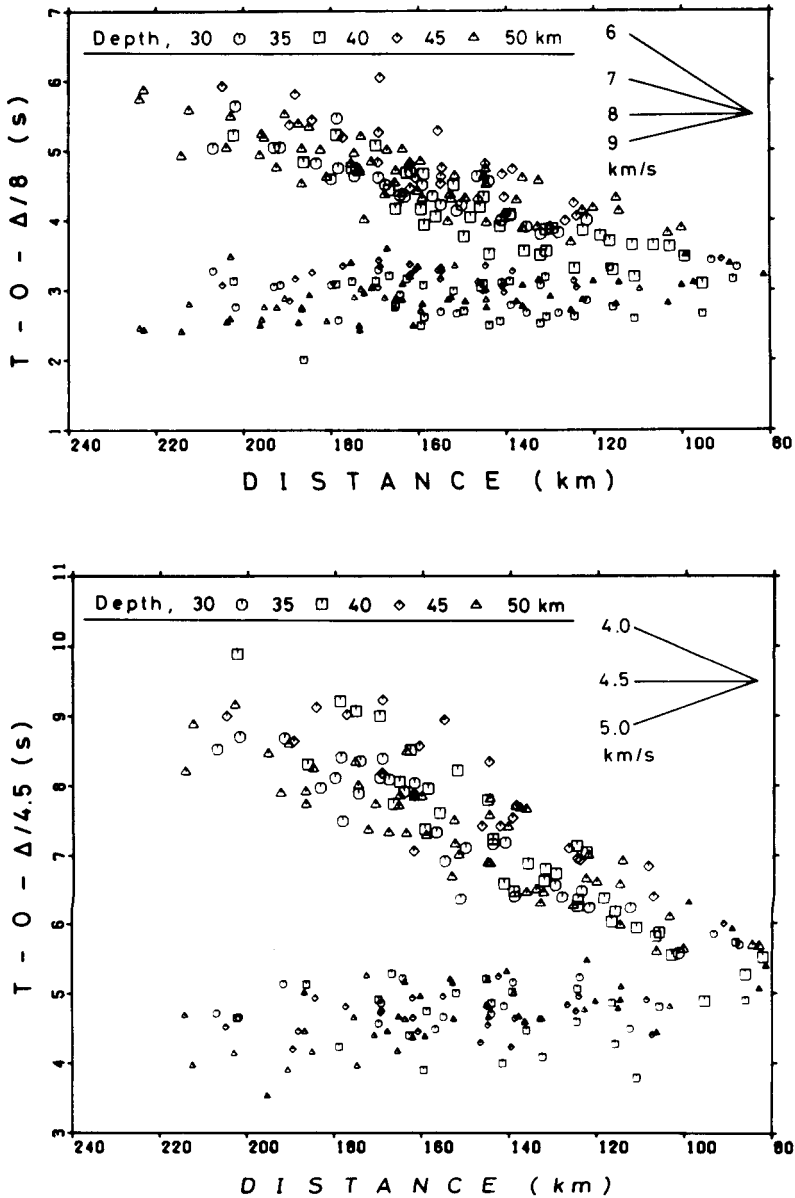
Figure 9. Composite travel-time plots of the initial and the later phases for case A. Small and large symbols indicate the initial and the later arrivals respectively. Different symbols indicate different focal depths. Top: *P*-waves; bottom: *S*-waves. No systematic dependence of the arrival times on the focal depths is recognized.

where i is the angle of a ray segment and v is the velocity (Eliseevnin 1965 in Julian & Gubbins 1977). The increments of emergent angle at the source are automatically adjusted during the calculation to obtain a sufficient density of travel-time plots on all branches and to obtain geometrical spreading in the x–z plane simultaneously. The amplitudes are calculated from geometrical spreading only. All other factors on the amplitudes and phase shifts, such as caustics, radiation patterns at the source and Q distribution, are not taken into account. These approximations do not critically affect our analysis because we mainly analyse travel times and

do not discuss the amplitudes quantitatively and the waveforms at all. Thus the simplest synthetic seismograms are obtained by superposition of wavelets whose onset times and amplitudes are calculated as described above.

We computed synthetic seismograms for a variety of structural models to search for the model that can explain the observation. After an extensive trial and error two different types of models remained. The first type is characterized by the Moho having a wedge or step between the source and the receiver. We call this type a 'wedge model'. A typical example of the wedge models and the result of the ray tracing calculation for it is shown in Fig. 10(a),
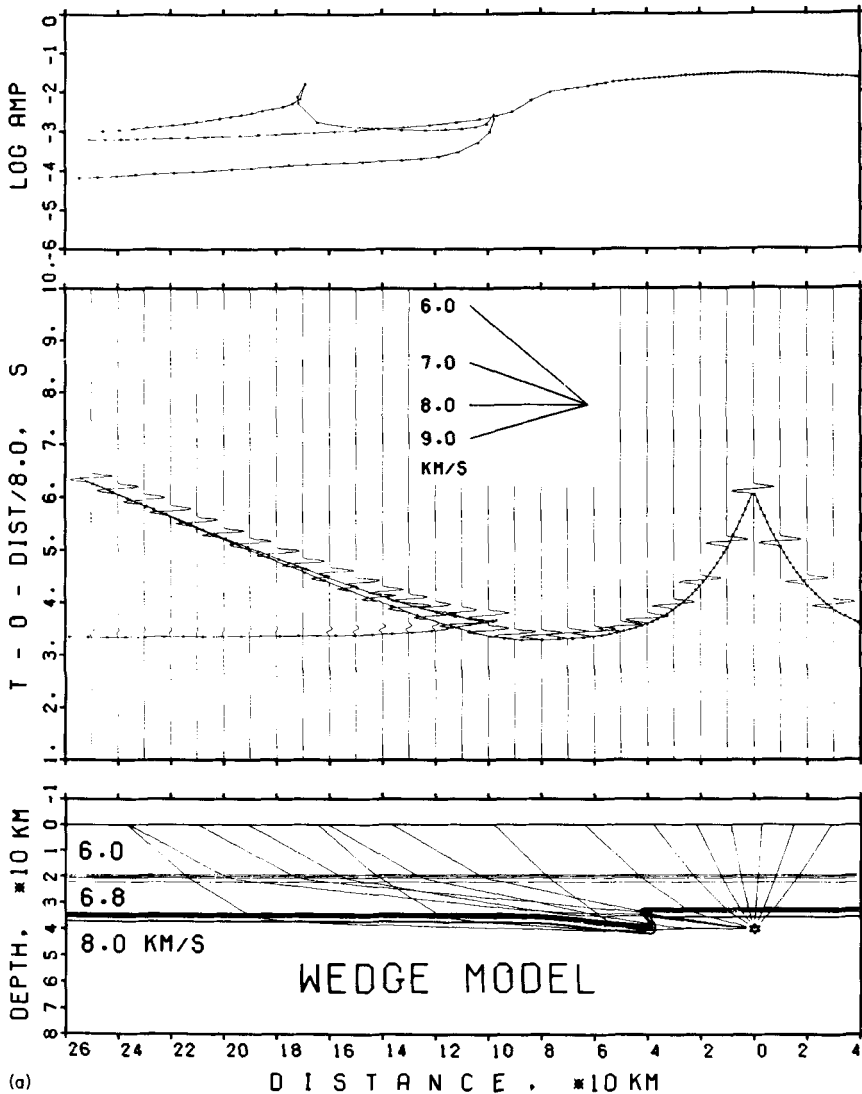
Figure 10. Typical example of the wedge model (a) and of the channel model (b) and the corresponding results of the ray tracing calculation. Top: amplitude curve. Middle: calculated travel-time curve and simple synthetic seismograms where the maximum amplitudes of all the seismograms are equalized. Bottom: velocity structure of the model expressed by the contour lines at intervals of $0.2 \, \mathrm{km \, s^{-1}}$. The focus and some of the calculated ray paths are also shown.
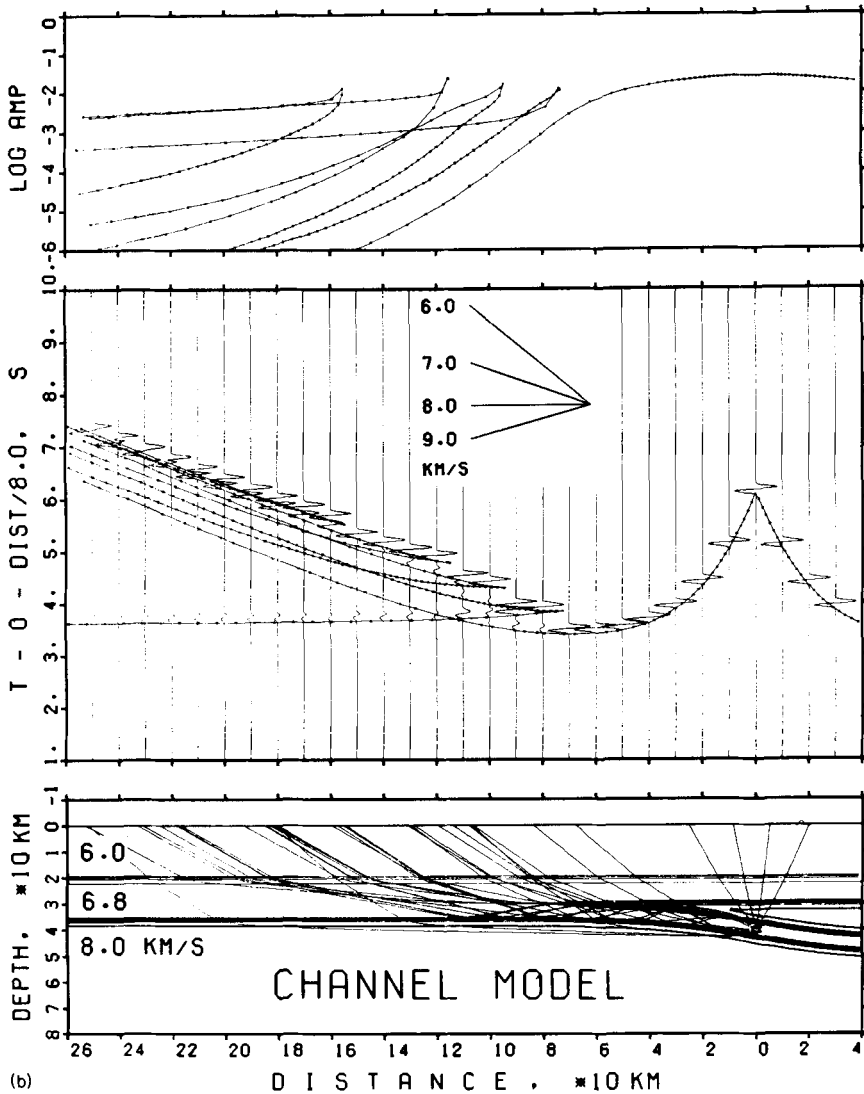
Figure 10 – *continued*

where the maximum amplitudes of all the seismograms are equalized. The later phase appears as the waves passing through the wedge and travelling in the lower crust almost horizontally. The amplitudes are large and the apparent velocities are nearly equal to the velocities of the lower crust.

The second type of the models is characterized by the hypocentres lying in a low-velocity channel that indents from the lower crust into the mantle. We call this type a 'channel model'. Fig. 10(b) shows a typical example of the channel models and the result of the ray tracing calculation for it. The seismic velocities of the channel are taken to be equal to those of the lower crust. The waves radiated relatively horizontally from a source are largely trapped in the channel and come up to the Earth's surface as multibranched later phases. The most energetic branches are those generated by the rays smoothly travelling in the channel. Other branches are formed by the multireflected rays travelling sinuously in the channel. They are

energetic only near the cusps. The later phases in this model, in general, last longer and are more complicated in waveform than those in a wedge model.

In paper I we proposed on heuristic grounds such a channel model that the subcrustal seismic zone constitutes a low-velocity channel which is a consequence of the subduction of the untransformed 'basaltic' oceanic crust into the mantle. We now present convicing evidence for preferring the channel model to the wedge model. The method to resolve these two types is to distinguish a 'station-common' apparent velocity from an 'event-common' apparent velocity. The latter is the apparent velocity in the ordinary definition. The former is obtained by plotting travel times against epicentral distances for a number of events observed at a certain station. This quantity has significance when the horizontal extent of the hypo-central distribution is sufficiently larger than the vertical one as in the present case. The 'station-common' apparent velocity is equivalent to the 'event-common' apparent velocity for a laterally homogeneous structure but not for a laterally heterogeneous structure. The 'station-common' apparent velocity indicated the speed of the waves propagating almost horizontally in the source region.

Fig. 11 illustrates schematically how the 'station-common' apparent velocity is different between two types of model. For a wedge model the 'station-common' apparent velocity must approximately agree with the mantle velocity for both the initial and the later phases because the source region lies in the mantle (Fig. 11a). On the other hand, for a channel model, this quantity approximately coincides with the mantle velocity for the initial phase but with the speed of the low-velocity channel for the later phase (Fig. 11b). Fig. 12 shows several examples of the 'station-common' travel-time plots for the initial and the later phases. As can
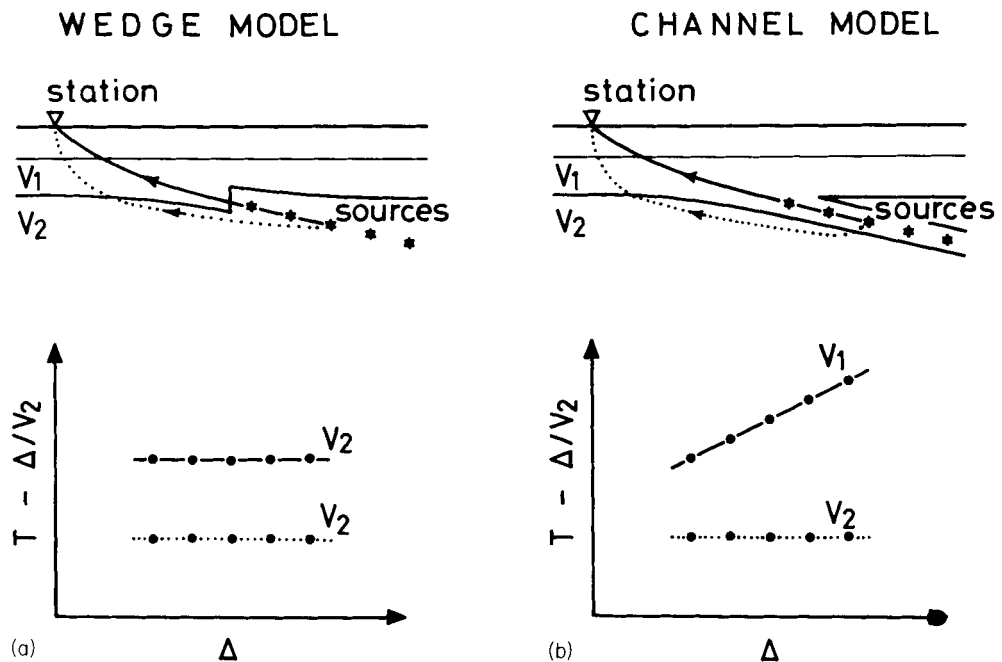
Figure 11. Schematic illustration showing the difference in 'station-common' travel-time plots between the wedge model (a) and the channel model (b). V1 and V2 represent the velocities of the lower crust (and the low-velocity channel) and of the sub-Moho mantle respectively. Dotted and solid curves correspond to the initial and later phases. The 'station-common' apparent velocities of the later phases almost coincide with V2 for the wedge model and with V1 for the channel model.
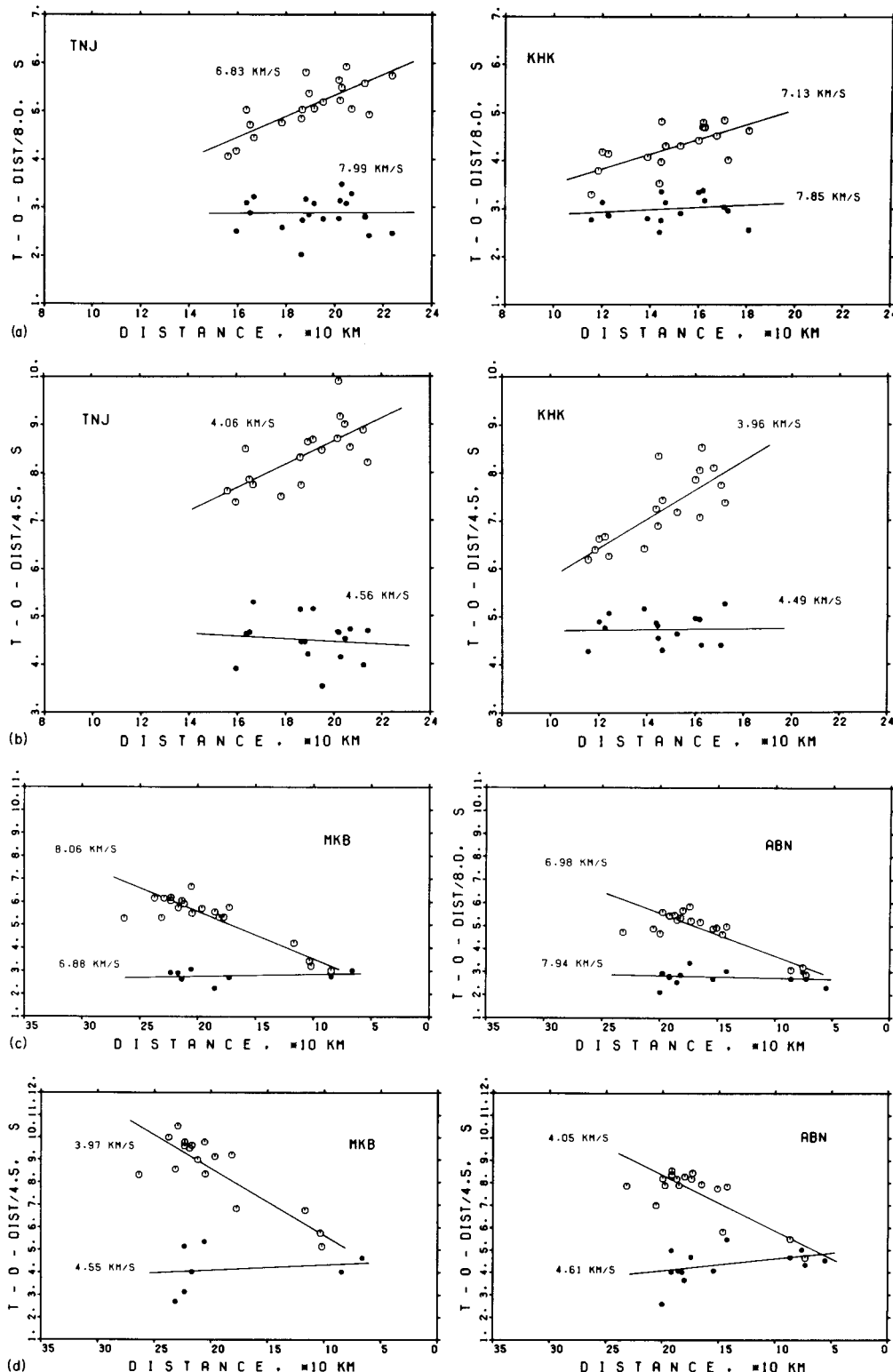
Figure 12. Examples of the 'station-common' travel-time plots. (a) *P*-waves for case A, (b) *S*-waves for case A, (c) *P*-waves for case B, (d) *S*-waves for case B. The initial and later arrivals are indicated by filled and open circles respectively. The solid line represents a least squares fit.

be seen, the 'station-common' apparent velocities of the P and S later phases are significantly lower than those of the P and S initial phases. This conclusion is not affected by possible systematic errors in hypocentral determination which affect only equally the measurements of the apparent velocities of the initial and the later phases. The significant difference in 'station-common' apparent velocity is consistent with the channel model but not with the wedge model. Table 3 lists the values of the 'station-common' apparent velocities and their weighted averages. Note that they approximately coincide with the 'event-common' apparent velocities obtained in the last section. The approximate coincidence for the later phases again supports the channel model against the wedge model. For a channel model, the 'station-common' apparent velocities of the initial and the later phases are approximately equal to the P and S velocities directly below the low-velocity channel and to the P and S velocities of the low-velocity channel itself respectively. The P and S velocities directly below the low-velocity channel are therefore 8.0–8.1 and 4.5–4.7 km s^{-1} which seem to be somewhat higher than the sub-Moho velocities (7.8–7.9 and 4.4–4.5 km s^{-1}) obtained for the relevant region by various authors (Aoki *et al.* 1972; Ikami 1978; Ukawa & Fukao 1982). The faster mantle below the low-velocity channel is also suggested from the ray-tracing analysis of the observed travel times as will be seen later. The P and S velocities of the low-velocity channel are on the other hand 6.8–6.9 and about 4.0 km s^{-1}, which approximately coincide with those of the lower crust estimated by several authors (e.g. Ukawa & Fukao 1982). We also note that these velocities are quite similar to those of the main layer of the oceanic crust (Christensen & Salisbury 1975; Hyndman 1979; Au & Clowes 1984).

The low-velocity channel is thus characterized by the seismic velocities of the 'basaltic' oceanic crust and the underlying mantle seems to be faster than the normal mantle, suggesting

Table 3. (a) 'Station-common' apparent velocities, case A.

Code	V1 km/s	N1	V2 km/s	N2	V3 km/s	N3	V4 km/s	N4
ABU	9.69+0.00	2	6.92+0.19	4	4.67+0.18	3	3.99+0.12	5
BHO	7.89+0.22	12	7.15+0.20	17	4.29+0.10	10	3.90+0.08	17
KGM	7.97+0.24	14	7.02+0.20	18	4.40+0.11	15	3.95+0.10	17
KHK	7.85+0.24	15	7.13+0.22	18	4.49+0.09	15	3.96+0.10	18
KTN	7.77+0.29	15	6.62+0.20	18	–	1	–	1
MYO	7.90+0.21	16	6.81+0.28	18	4.64+0.18	11	3.94+0.10	16
OHM	–	1	–	1	4.46+0.13	12	4.02+0.08	18
RKO	–	1	6.70+0.00	2	–	0	–	0
TNJ	7.99+0.28	19	6.83+0.18	20	4.56+0.13	17	4.06+0.09	18
UJI	9.10+0.76	4	7.00+0.20	6	–	1	–	1
WTJ	12.93+0.00	2	8.05+0.00	2	–	0	–	0
YGI	7.85+0.22	18	7.06+0.17	20	4.44+0.10	14	3.96+0.12	19
AVRG	7.95+0.31		6.94+0.18		4.48+0.09		3.97+0.05	

Explanations are the same as in Table 2(a).

(b) 'Station-common' apparent velocities, case B.

| Code	V1 km/s	N1	V2 km/s	N2	V3 km/s	N3	V4 km/s	N4
ABN	7.94+0.10	13	6.98+0.11	20	4.61+0.07	13	4.05+0.07	17
CHT	7.88+0.06	14	7.36+0.30	16	4.37+0.07	5	4.17+0.07	14
KGW	8.70+0.34	12	6.89+0.07	18	5.62+1.67	5	3.91+0.06	15
MIK	8.12+0.11	7	6.96+0.10	21	4.67+0.09	7	3.93+0.07	19
MKB	8.06+0.10	8	6.88+0.09	20	4.55+0.10	7	3.97+0.06	17
MZI	8.81+0.25	14	6.64+0.11	21	5.67+2.12	4	3.91+0.05	19
OKB	7.10+0.28	12	6.76+0.11	15	5.29+0.80	6	3.91+0.06	14
SIZ	7.12+0.36	9	6.47+0.20	10	5.57+0.70	5	4.73+0.34	9
TNR	8.09+0.16	13	6.75+0.09	21	5.53+0.68	7	3.87+0.05	19
AVRG	8.07+0.45		6.84+0.17		4.72+0.31		3.97+0.13	

Explanations are the same as in Table 2(a).

that they constitute the subducting part of the oceanic lithosphere. Its crustal portion remains as of a basaltic mineral assemblage at depths below the continental Moho. The basalt–eclogite transformation does not seem to occur at least down to depths of 50–60 km. The argument developed above thus strongly supports the earlier conclusion derived in paper I that the subcrustal seismic zone manifests the untransformed 'basaltic' oceanic crust subducted into the mantle and that the later phases are generated within it.

There are two alternative explanations as to why distinct later phases are not observed for events deeper than 60 km. First, basalt may transform into eclogite at depths near 60 km so that the subducting oceanic crust would no longer be a low-velocity zone at greater depths. Fig. 8 in this case indicates that the transformation from basalt to eclogite is quite sharp. Second, the untransformed oceanic crust may extend further below 60 km but earthquakes at greater depths occur outside and perhaps below it. At present, it is difficult to resolve these two alternatives.

5 Model construction

In this section, we construct a quantitative channel model that explains the observed travel times, taking into account the crustal and subcrustal structural models so far presented. For this purpose we use again the method of 2-D ray tracing. Admittedly the method cannot help us to make complete models because of the three-dimensionality of the problem. We will obtain the approximate models along the profiles shown by the solid arrows in Fig. 5. We will make ray tracing simulations for a source placed at a position averaged over the hypocentres of all the events. The results will be compared with the composite travel-time data. Before comparison, however, a correction must be made for the travel-time data. The hypocentral parameters routinely determined were for the models without a low-velocity channel in the mantle. Introduction of a low-velocity channel would slightly shift the origin time earlier and the hypocentre deeper. Provided that the source is situated in just the middle of the oceanic crust with a thickness of 6 km, the shift of an origin time is roughly estimated at 0.3 s and the shift of a focal depth at 2 km. We corrected the hypocentral parameters with these values for all the events prior to the model construction.

The model is made up of several homogeneous layers with variable thicknesses. The continental crust consists of the surface layer, the upper crust and the lower crust. The oceanic plate consists of the oceanic crust and the lithospheric mantle. The boundaries between the adjacent layers are represented by steep transition zones with thicknesses of about 1 km. The P velocities of the crust and the sub-Moho mantle and the Moho depth are given as in Figs 13 and 15 by referring to those routinely used in the hypocentral determinations which were derived from the travel-time analyses of either explosions or earthquakes (Aoki *et al.* 1972; Kanamori & Tsumura 1971). A deep Conrad discontinuity in the eastern region is required
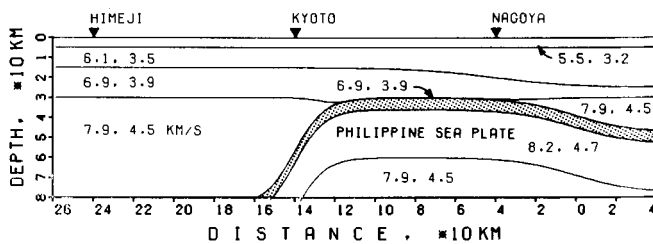
Figure 13. The velocity structure model for case A (profile along the solid arrow A in Fig. 5). Numbers in each layer indicate V_P and V_S (km s^{-1}). The oceanic crust is indicated by stippling.

from a refraction study (Aoki *et al.* 1972). The corresponding *S* velocities are determined on the basis of the *S* to *P* ratio studies of Ukawa & Fukao (1981). The subducting oceanic crust is delineated by the subcrustal seismic zone so that it passes through the representative source placed at a depth of 42 km (case A) and 44 km (case B) and comes in touch with the continental Moho midway between the source and the distant receivers. The oceanic crust is assumed to have a typical thickness of 6 km. Note that Ukawa (1982) estimated the thickness of the subcrustal seismic zone to be about the same, 7 km. The thickness of the whole oceanic plate is assumed to be 30 km (Kanamori & Abe 1968), although the waves we are concerned with graze through only the sub-Moho part of the subducting plate so that the deeper part cannot be resolved.

Fig. 13 shows the final model for case A. The *P*- and *S*-wave velocities of the subducting
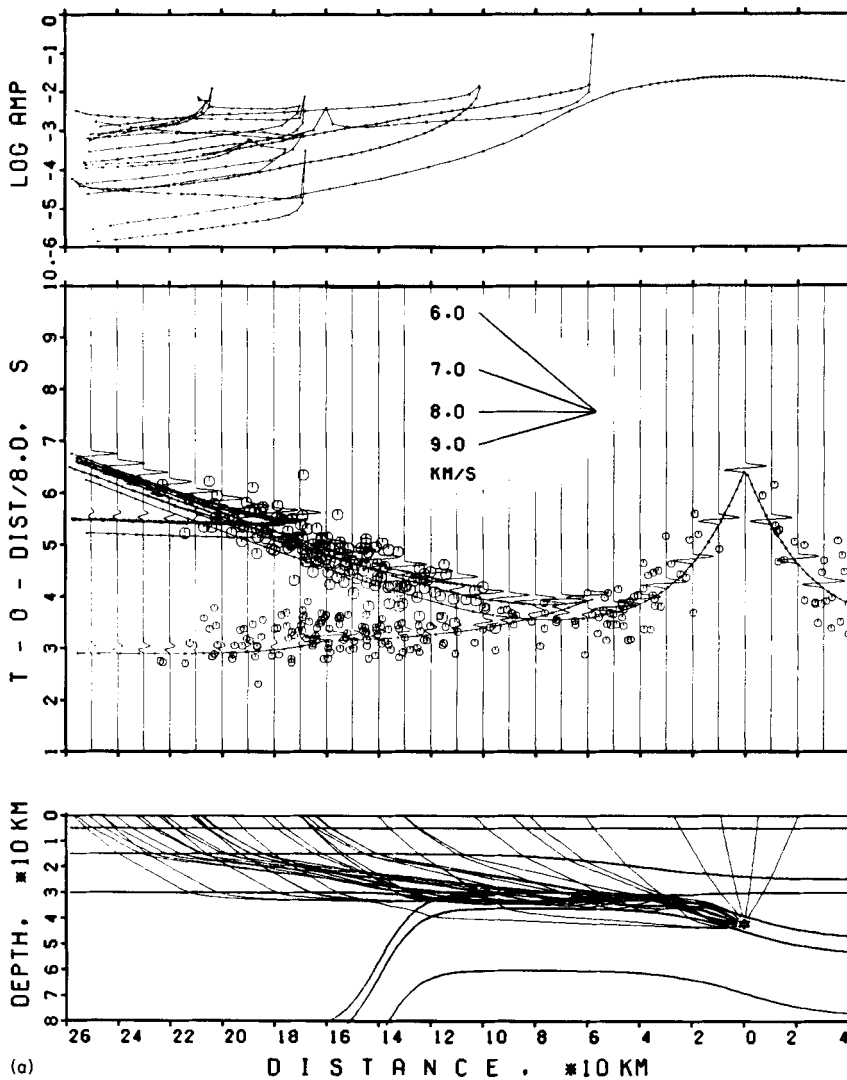
Figure 14. The result of ray tracing calculation for the velocity structure model shown in Fig. 13. (a) *P*-waves, (b) *S*-waves. Observed arrival times of the initial and the later phases (composite) are indicated by small and large open circles respectively. See Fig. 10 for other explanation.
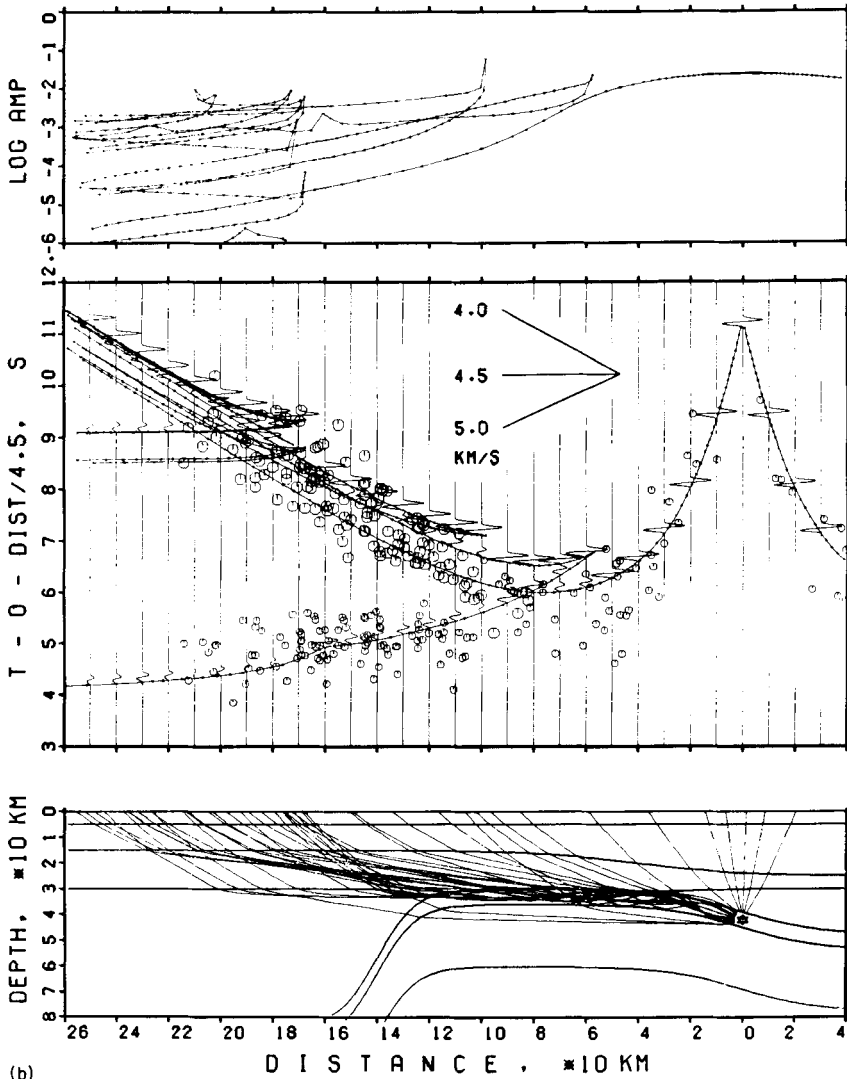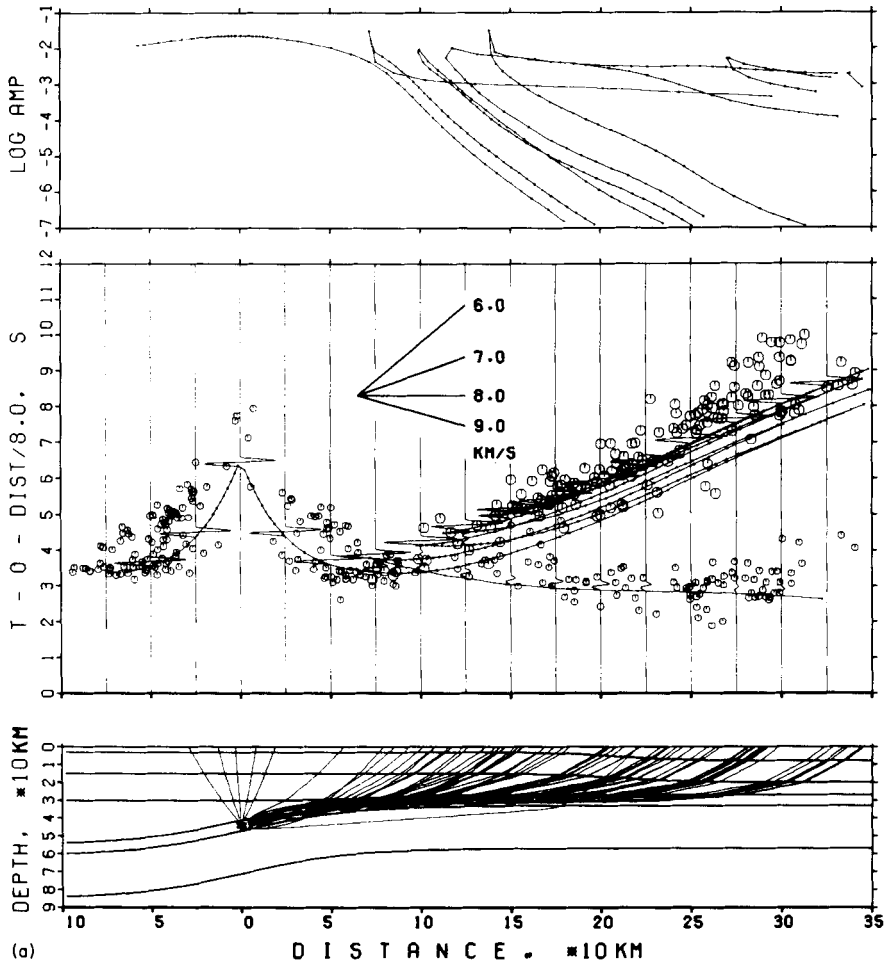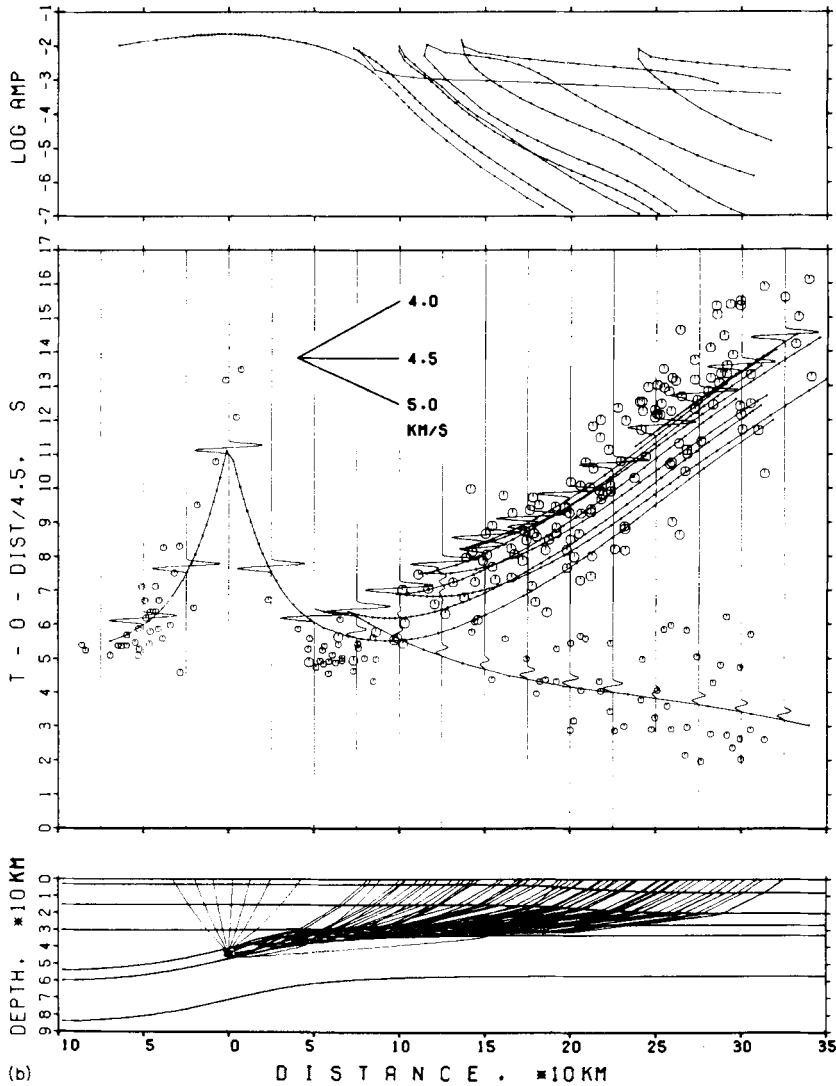
Figure 14 – *continued*

oceanic mantle are determined to be 8.2 and 4.7 km s^{-1} respectively. Such high velocities are required to explain the observed travel times of the initial phases. The depth of the Conrad discontinuity in the western region has not yet been determined accurately. We tentatively place this discontinuity at a depth of 15 km to explain the travel times of the later phases. Then the apparent velocities of the later phases require that the P and S velocities of the subducting oceanic crust (and the continental lower crust) be about 6.9 and 3.9 km s^{-1} respectively. We sharply bent downwards the model subducting slab at the western periphery of Lake Biwa because some kind of truncation is suggested there from the seismicity. Our analysis is little affected by the detailed method of truncation. Fig. 14(a) shows the result of the ray tracing simulation for the P-wave velocity model. The composite data of the observed travel times are superimposed in the middle figure where the first and the later arrivals are denoted by the small and the large circles respectively. The figure shows a good agreement
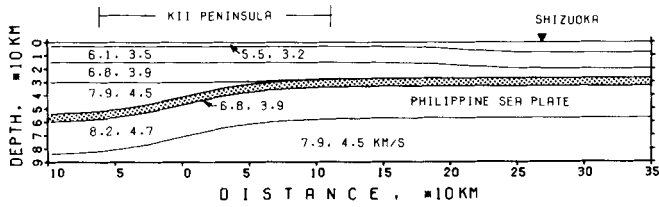
Figure 15. The velocity structure model for case B (profile along the solid arrow B in Fig. 5). See Fig. 13 for the explanation.

between the observation and the calculation. Fig. 14(b) shows the results for the S-wave velocity model. The agreement is as good as for the P-wave model.

Fig. 15 shows the model for case B. The results of the ray tracing for the P- and S-wave velocity models are shown in Figs. 16(a) and (b) respectively. The velocities of the subducting oceanic mantle are equal to those in case A. In our interpretation the lower crust in the

Figure 16. The result of ray tracing calculation for the velocity structure model shown in Fig. 15. (a) P-waves, (b) S-waves. See Figs 10 and 14 for the explanation.

Figure 16 – *continued*

eastern part of the profile is in direct contact with the subducting oceanic crust so that the Moho in this region is the 'oceanic Moho'. This Moho is placed at a depth of 33 km based on the crustal model of Ikami (1978). The surface 'sedimentary' layer is thickened eastward because of the thick sediments of the Cretaceous and the later eras. Such thickening of the sedimentary layer (Ikami 1978) explains well rather low values of apparent velocities for the later phases as compared with those in case A.

Thus, our basic idea described in the last section is now shown to be 'quantitatively' consistent with the observed travel times and to be reasonably matched with the crustal models so far presented. Admittedly the two models obtained in this section are not unique and the detail would have to be revised with the addition of data.

6 Discussion and conclusion

We found that there lies a low-velocity layer ($V_P \simeq 7\,\mathrm{km\,s^{-1}}$, $V_S \simeq 4\,\mathrm{km\,s^{-1}}$) in the mantle beneath the Chubu district and the Kii peninsula. Seismic waves primarily trapped in this layer make their apperance on seismograms at particular stations as prominent later phases. The low-velocity layer is interpreted as the untransformed oceanic crust at the top of the Philippine Sea plate subducting beneath this region. The results of the analysis are summarized as follows:

(i) The oceanic crust descending into the mantle remains basaltic at least down to depths of 50–60 km. Transformation from basalt to eclogite must take place at further depths.

(ii) Subcrustal earthquakes shallower than 50–60 km are occurring within the subducted oceanic crust.

According to the pressure–temperature stability diagram and the shear stress heating curves for crustal elements (Turcotte & Schubert 1973), a layer of crustal basalt and gabbro attached to the upper surface of a lithospheric slab will enter into the stability field of eclogite at depths shallower than 20–30 km upon subduction (Ahrens & Schubert 1975). However, at these depths the temperature of crustal elements will not exceed 200°C (Turcotte & Schubert 1973) and the reaction rate may be sufficiently slow for basalt to be metastable well into the eclogite stability field. The transition from basalt to eclogite in the relatively cold descending crust is, thus, a rate-dominated process.

Convergence rate of the Philippine Sea plate is estimated to be 40 mm yr^{-1} towards the NW (Seno 1977; Minster & Jordan 1978). The vertical rate is estimated at 10 mm yr^{-1}, taking the dip angle of the slab into account. Suppose that basaltic elements in the oceanic crust go into the eclogite stability field at a depth of 20 km. The results of our analysis suggest that these elements remain without transformation for a subsequent period of more than 3×10^6 yr down to a depth of 50 km. It is possible from this to constrain the temperature of the descending oceanic crust assuming that the temperature is a dominant factor for the transformation. Ito & Kennedy (1971) investigated the basalt–eclogite reaction rate as a function of temperature. According to them basalt completely transforms to eclogite in 5 min at 1200°C and in a week or more at 800°C. At temperatures as low as 400°C geologic times of 10^6–10^7 yr would be required for the transformation. These numbers suggest that the temperature of the descending oceanic crust is not more than 400–500°C at a depth of about 50 km.

The basaltic portion of the subducted oceanic crust strongly affects the driving force of the oceanic lithosphere. The buoyancy force per unit area acting on the oceanic lithosphere subducted into the asthenosphere at a gentle dip is roughly given by $(h_c \Delta \varrho_c - h_m \Delta \varrho_m)g$, where h, g and $\Delta \varrho$ are the lithospheric thickness, the gravitational acceleration and the density difference relative to the asthenospheric material. Subscripts c and m are the crustal and mantle parts of the oceanic lithosphere. The Philippine Sea plate in the relevant region is young (20–30 Myr from magnetic lineation – Kobayashi & Nakada 1978) so that the mantle portion would be relatively thin. If we take $\Delta \varrho_m = 50\,\mathrm{kg\,m^{-3}}$, $h_c = 6 \times 10^3$ m and $h_c + h_m = 3 \times 10^4$ m (Kanamori & Abe 1968), we obtain a positive buoyancy force of 1.5×10^7 N m^{-2} for the plate with 'basaltic' oceanic crust ($\Delta \varrho_c = -450\,\mathrm{kg\,m^{-3}}$), and a negative buoyancy force of 2.1×10^7 N m^{-2} for the plate with 'eclogitic' oceanic crust ($\Delta \varrho_c = 150\,\mathrm{kg\,m^{-3}}$). Consequently, the Philippine Sea plate subducting beneath SW Japan is still buoyant down to depths of at least 50 km. As pointed out by Sacks (1983), the positive buoyancy due to the light untransformed oceanic crust is likely to affect the subduction geometry. On one hand, it is very unlikely that the slab pull due to the excess weight of the subducted portion of the oceanic lithosphere drives the subducting motion of the Philippine

Sea plate along the Nankai–Suruga trough if its leading edge only reaches a depth of 60–80 km as suggested by the seismicity. Ruff & Kanamori (1983) also referred to the basalt–eclogite transition depth. They pointed out that the subducting and the overlying plate seem to be seismically uncoupled below 40 km. They attributed the uncoupling to the basalt–eclogite transformational superplasticity. Alternatively we may attribute the seismic coupling and uncoupling to the difference in buoyancy; the positive buoyancy acting on the subducting plate strengthens the coupling and the negative buoyancy weakens it.

The subcrustal seismic zone is located at depths of 20–30 km in the coastal region of the Chubu district, where the upper crust is much thinner than that further inland (Aoki *et al.* 1972), reflecting the transitional nature of the coastal region from continent to ocean. The crustal model derived from explosion observations (Ikami 1978), however, does not show a seaward shallowing of the Moho so that the lower crust is thickened oceanwards in the coastal region. In our interpretation this thickening of the lower crust is a consequence of the contact of the subducting oceanic crust with the original continental lower crust which is hard to distinguish in terms of seismic velocities. Therefore the Moho observed beneath the coastal region represents the bottom of the 'oceanic' crust.

As described in Section 2, the subcrustal seismic zone raises itself in a narrow region extending north-westwards from Ise Bay to Lake Biwa. Mizoue (1971), Yoshii *et al.* (1974) and Hurukawa (1983) have shown that the Moho in this region lies at a depth of 35–40 km, about 5–10 km deeper than the Moho in the surrounding area. This crustal thickening can also be interpreted as an overlap of the continental and the oceanic crusts. Gravity surveys have revealed a prominent negative Bouguer anomaly around this area (Hagiwara 1967). Fig. 17 shows the Bouguer anomaly map with $0.05 \, \text{mm s}^{-2}$ contour (after Shiraki *et al.*, in preparation) and the gravity profile along the line corresponding approximately to the solid arrow A in Fig. 5. In the bottom illustration of Fig. 17 the short-wavelength anomalies (indicated by hachures) are largely attributed to shallow sediments. The remaining long-wavelength negative anomaly of the amplitude of 0.25–$0.3 \, \text{mm s}^{-2}$ is difficult to interpret by shallow sediments (Shiraki *et al.*, in preparation). This long-wavelength anomaly has been interpreted as a locally thickened continental crust (Hurukawa 1983). However, this anomaly is also consistent, at least qualitatively, with our model. As shown below, the existence of the oceanic lithosphere close to the Earth's surface does not necessarily cause a 'positive' gravity anomaly. Referring to the subcrustal seismicity, we approximate the 2-D configuration of the subducted lithosphere along profile AB in Fig. 17 by a sinusoidal wave with a wavelength L ($=200 \, \text{km}$) and a total amplitude A ($=20 \, \text{km}$). The resultant maximum Bouguer anomaly is then roughly given by

$$2 \, GA \exp\left(-2\pi D/L\right)\left[\Delta\varrho_c + (\Delta\varrho_m - \Delta\varrho_c) \exp\left(-2\pi h_c/L\right) - \Delta\varrho_m \exp\left(-2\pi(h_c + h_m)/L\right)\right]$$

where G is the gravitational constant and D ($=40 \, \text{km}$) is the characteristic depth of the upper surface of the subducted lithosphere which undulates between depths 30 and 50 km. For the density values of $\Delta\varrho_c = -450 \, \text{kg m}^{-3}$ and $\Delta\varrho_m = 50 \, \text{kg m}^{-3}$, we expect a 'negative' Bouguer anomaly with a minimum value of $-0.13 \, \text{mm s}^{-2}$ above the subducted lithosphere. The spatial pattern of Bouguer anomaly is consistent with the observation. The observed amplitude is, however, twice as large as the calculated one. We do not consider that this difference is serious as the model is too simple and the gravity reductions for sediments are highly uncertain. We also point out the possibility of the presence of an eclogitic oceanic crust at depths greater than 50–60 km which may cause a positive Bouguer anomaly. With this possibility the expected negative anomaly would become much larger than indicated by the above calculation. What is important here is to recognize that the subducted oceanic lithosphere immediately below the

7
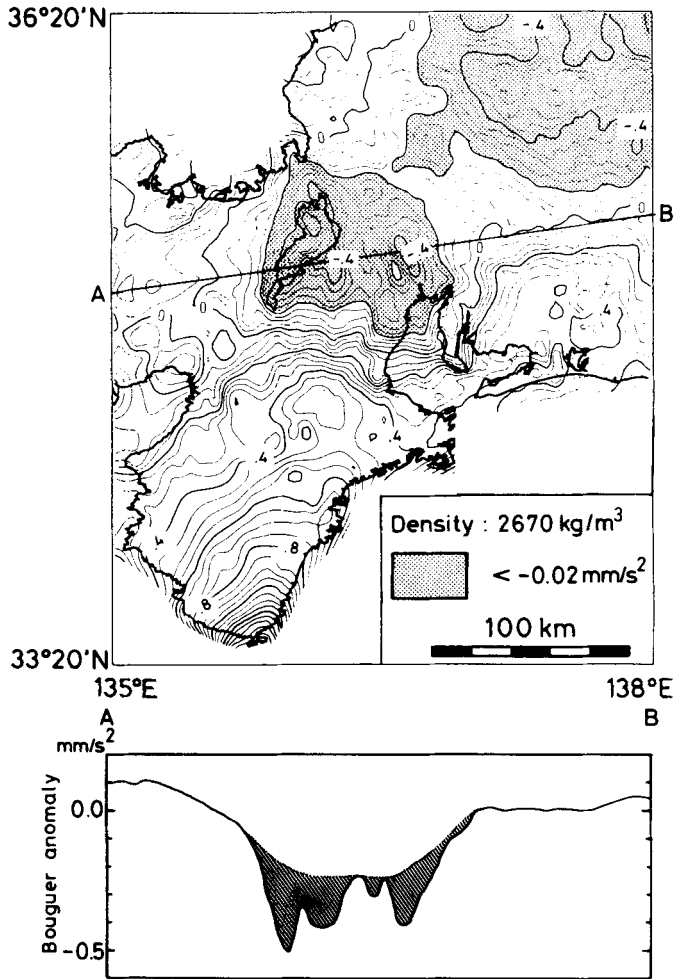
Figure 17. Top: Bouguer anomaly map with $0.05\,\mathrm{mm\,s^{-2}}$ contour in central Japan (after Shiraki *et al.*, in preparation). Stippling indicates areas of Bouguer low ($< -0.2\,\mathrm{mm\,s^{-2}}$). The line AB appears in the bottom illustration. Bottom: gravity profile along the solid line AB. The short-wavelength anomaly indicated by hachures is presumably due to the effect of shallow sediments. The remaining long-wavelength anomaly cannot be attributed to such an effect (Shiraki *et al.*, in preparation).

Moho causes a 'negative' gravity anomaly rather than a 'positive' anomaly. As for the configuration of the subducted Philippine Sea plate, it is still puzzling why the subducting slab is indented inland, keeping its top in contact with the bottom of the continental crust. The trench axis of the Nankai–Suruga trough does not exhibit a distinct bend at the corresponding position.

S to *P* converted phases were reported for deep events in the Chubu districts by Suganuma *et al.* (in Ukawa 1982). According to them there are two conversion interfaces corresponding to the Conrad discontinuity and the subcrustal seismic zone. A reasonable explanation for the latter conversion is provided by our model where the seismic zone is a thin and distinct low-velocity layer in the mantle. *ScS* to *P* phase conversion observed in the Chugoku and the Shikoku districts, to the west of the Kinki district (Nakanishi 1980), may also be explained in terms of the untransformed oceanic crust.

Our model is thus consistent with and supported by other geophysical evidence but several questions are still unresolved. Does the oceanic crust subduct down to further depths beyond 50–60 km without transformation? Is it possible to observe a similar feature in other subduction zones? Why are the earthquakes in this region restricted within the crustal part of the oceanic lithosphere? These are subjects beyond our scope and further work needs to be done.

References

Ahrens, T. J. & Schubert, G., 1975. Gabbro-eclogite reaction rate and its geophysical significance, *Rev. Geophys. Space Phys.*, **13**, 383–400.

Aki, K., 1961. Crustal structure in Japan from the phase velocity of Rayleigh waves, Part 1. Use of the network of seismological stations operated by the Japan Meteorological Agency, *Bull. Earthq. Res. Inst., Univ. Tokyo*, **39**, 255–283.

Ando, M., 1975. Source mechanisms and tectonic significance of historical earthquakes along the Nankai trough, Japan, *Tectonophys.*, **27**, 119–140.

Aoki, H., 1980. Deep seismic zone to the west of Suruga Bay, central Japan, *Proc. Symp. Earthquake Prediction Research*, pp. 97–107 (in Japanese).

Aoki, H., Tada, T., Sasaki, Y., Ooida, T., Muramatu, I., Shimamura, T. & Furuya, I., 1972. Crustal structure in the profile across central Japan as derived from explosion seismic observations, *J. Phys. Earth*, **20**, 197–223.

Au, D. & Clowes, R. M., 1984. Shear-wave velocity structure of the oceanic lithosphere from ocean bottom seismometer studies, *Geophys. J. R. astr. Soc.*, **77**, 105–123.

Christensen, N. I., 1972. Compressional and shear wave velocities at pressure to 10 kilobars for basalts from the East Pacific Rise, *Geophys. J. R. astr. Soc.*, **28**, 425–429.

Christensen, N. I. & Salisbury, M. H., 1975. Structure and constitution of the lower oceanic crust, *Rev. Geophys. Space Phys.*, **13**, 57–86.

Cohen, L. H., Ito, K. & Kennedy, G. C., 1967. Melting and phase relations in an anhydrous basalt to 40 kilobars, *Am. J. Sci.*, **265**, 475–518.

Delany, J. M. & Helgeson, H. C., 1978. Calculation of the thermodynamic consequences of dehydration in subducting oceanic crust to 100 km and >800°C, *Am. J. Sci.*, **278**, 638–686.

Engel, A. E. J. & Engel, G. C., 1964. Composition of basalt from the mid-Atlantic ridge, *Science*, **144**, 1330–1333.

Fitch, T. J. & Scholz, C. H., 1971. Mechanism of underthrusting in southwest Japan: a model of convergent plate interiors, *J. geophys. Res.*, **76**, 7260–7292.

Fukao, Y., Hori, S. & Ukawa, M., 1983. A seismological constraint on the depth of basalt-eclogite transition in a subducting oceanic crust, *Nature*, **303**, 413–415.

Gebrande, H., 1976. A seismic ray tracing method for two-dimensional inhomogeneous media, in *Explosion Seismology in Central Europe*, pp. 162–167, Springer-Verlag, Berlin.

Green, D. H. & Ringwood, A. E., 1972. A composition of recent experimental data on gabbro-garnet granulite-eclogite transition, *J. Geol.*, **80**, 277–288.

Hagiwara, Y., 1967. Analysis of gravity values in Japan, *Bull. Earthq. Res. Inst., Univ. Tokyo*, **45**, 1081–1228.

Hashimoto, M., 1982. Numerical modelling of the three-dimensional stress field in southwestern Japan, *Tectonophys.*, **84**, 247–266.

Hurukawa, N., 1983. P_n velocity and Moho-offset at the west of Lake Biwa in the Kinki district, Japan, *J. Phys. Earth*, **31**, 33–46.

Hyndman, R. D., 1979. Poisson's ratio in the oceanic crust – a review, *Tectonophys.*, **59**, 321–333.

Ikami, A., 1978. Crustal structure in the Shizuoka district, central Japan, as derived from explosion seismic observations, *J. Phys. Earth*, **26**, 299–331.

Inoue, H. & Fukao, Y., 1984. An algorithm of two-dimensional seismic ray tracing, *Prog. Abstr., Seism. Soc. Japan, No. 1,* B76 (in Japanese).

Ito, K., 1977. Prominent phases from subcrustal earthquakes and crustal structure in the northern Kinki district, Japan, *Prog. Abstr., Seism. Soc. Japan. No. 2,* 330 (in Japanese).

Ito, K. & Kennedy, G. C., 1971. An experimental study of the basalt-garnet granulite-eclogite transition, *Geophys. Monogr. Am. geophys. Un.*, **14**, 303–314, Washington, DC.

Julian, B. R. & Gubbins, D., 1977. Three-dimensional seismic ray tracing, *J. Geophys.*, **43**, 95–113.

Kaminuma, K., 1966a. The crustal and upper mantle structure in Japan, Part 1. Phase velocities of Love and Rayleigh waves in central Japan, *Bull. Earthq. Res. Inst., Univ. Tokyo*, **44**, 481–494.

Kaminuma, K., 1966b. The crust and upper mantle structure in Japan, Part 2. Crustal structure in Japan from the phase velocity of Rayleigh waves, *Bull. Earthq. Res. Inst., Univ. Tokyo*, **48**, 495–510.

Kanamori, H., 1963a. Study on the crust–mantle structure in Japan. Part 1. Analysis of gravity data, *Bull. Earthq. Res. Inst., Univ. Tokyo*, **41**, 743–759.

Kanamori, H., 1963b. Study on the crust-mantle structure in Japan. Part 2. Interpretation of the results obtained by seismic refraction studies in connection with the study of gravity and laboratory experiments, *Bull. Earthq. Res. Inst., Univ. Tokyo*, **41**, 761–779.

Kanamori, H., 1972a. Relation between tectonic stress, great earthquakes and earthquake swarm, *Tectonophys.*, **14**, 1–12.

Kanamori, H., 1972b. Tectonic implication of the 1944 Tonanki and 1946 Nankaido earthquakes, *Phys. Earth planet. Int.*, **5**, 129–139.

Kanamori, H. & Abe, K., 1968. Deep structure of island arcs revealed by surface wave studies, *Bull. Earthq. Res. Inst., Univ. Tokyo*, **46**, 1001–1025.

Kanamori, H. & Tsumura, K., 1971. Spatial distribution of earthquakes in the Kii peninsula, Japan, south of Median Tectonic Line, *Tectonophys.*, **12**, 327–342.

Kay, R., Hubbard, N. J. & Gast, P., 1970. Chemical characteristics and origin of oceanic ridge volcanic rocks, *J. geophys. Res.*, **75**, 1581–1613.

Kobayashi, K. & Nakada, M., 1978. Magnetic anomalies and tectonic evolution of the Shikoku Inter-arc Basin, *J. Phys. Earth*, **26**, S391–S402.

Langston, C. A., 1981. Evidence for the subducting lithosphere under southern Vancouver Island and western Oregon from teleseismic *P* wave conversions, *J. geophys. Res.*, **86**, 3857–3866.

Manghani, M. H., Ramananantoandro, R. & Clark, S. P. (Jr), 1974. Compressional and shear wave velocities in granulite facies rocks and eclogites to 10 kbar, *J. geophys. Res.*, **79**, 5427–5446.

McConnell, R. K. (Jr), Gupta, R. N. & Wilson, J. T., 1966. Complication of deep crustal seismic refraction profiles, *Rev. Geophys. Space Phys.*, **4**, 41–100.

Mikumo, T., 1966. A study on crustal structure in Japan by the use of seismic and gravity data, *Bull. Earthq. Res. Inst., Univ. Tokyo*, **49**, 33–62.

Minster, J. B. & Jordan, T. H., 1978. Present-day plate motions, *J. geophys. Res.*, **83**, 5331–5354.

Mizoue, M., 1971. Crustal structure from travel times of reflected and refracted seismic waves recorded at Wakayama Microearthquake Observatory and its substations, *Bull. Earthq. Res. Inst., Univ. Tokyo*, **49**, 33–62.

Mizoue, M., 1977. Some remarks on the characteristics of subcrustal earthquake activities, in *Proc. Symp. Earthquake Prediction Research*, pp. 97–105 (in Japanese).

Mizoue, M., Nakamura, M., Seto, N. & Ishiketa, Y., 1983. Three-layered distribution of microearthquakes in relation to focal mechanism variation in the Kii peninsula, southwestern Honshu, Japan, *Bull. Earthq. Res. Inst., Univ. Tokyo*, **58**, 287–310.

Nakanishi, I., 1980. Precursors to *ScS* phases and dipping interface in the upper mantle beneath southwestern Japan, *Tectonophys.*, **69**, 1–35.

Nakanishi, I., Suyehiro, K. & Yokota, T., 1981. Regional variations of amplitudes of *ScSp* phases observed in the Japanese Islands, *Geophys. J. R. astr. Soc.*, **67**, 615–634.

Okada, H., 1979. New evidence of the discontinuous structure of the descending lithosphere as related by *ScSp* phases, *Suppl. J. Phys. Earth*, **27**, S53–S63.

Ringwood, A. E., 1972. Phase transformation and mantle dynamics, *Earth planet. Sci. Lett.*, **14**, 233–241.

Ringwood, A. E., 1974. The petrological evolution of island arc systems, *J. geol. Soc. London*, **130**, 183–204.

Ringwood, A. E., 1975. *Composition and Petrology of the Earth's Mantle*, McGraw-Hill, New York.

Ringwood, A. E., 1976. Phase transformations in descending plates and implications for mantle dynamics, *Tectonophys.*, **32,** 129–143.

Ringwood, A. E. & Green, D. H., 1966. An experimental investigation of the gabbro–eclogite transition and some geophysical implications, *Tectonophys.*, **3,** 383–427.

Ruff, L. & Kanamori, H., 1983. Seismic coupling and uncoupling at subduction zones, *Tectonophys.*, **99,** 99–117.

Sacks, I. S., 1983. The subduction of young lithosphere, *J. geophys. Res.*, **88,** 3355–3366.

Seno, T., 1977. The instantaneous rotation vector of the Philippine Sea plate relative to the Eurasian plate, *Tectonophys.*, **42,** 209–226.

Shiono, K., 1977. Focal mechanisms of major earthquakes in southwestern Japan and their tectonic significance, *J. Phys. Earth*, **28,** 17–44.

Shor, G. G. (Jr), Dehlinger, P., Kirk, H. K. & French, W. S., 1968. Seismic refraction studies off Oregon and northern California, *J. geophys. Res.*, **73,** 2173–2194.

Turcotte, D. L., & Schubert, G. C., 1973. Frictional heating of the descending lithosphere, *J. geophys. Res.*, **78,** 5876–5886.

Ukawa, M., 1982. Lateral stretching of the Philippine Sea plate subducting along the Nankai-Suruga trough, *Tectonics*, **1,** 543–571.

Ukawa, M. & Fukao, Y., 1981. Poisson's ratio of the upper and lower crust and the sub-Moho mantle beneath central Honshu, Japan, *Tectonophys.*, **77,** 233–256.

Ukawa, M. & Fukao, Y., 1982. Simultaneous determination of P and S velocities of the crust and the sub-Moho mantle with earthquake hypocenters in central Honshu, Japan, *J. Phys. Earth*, **30,** 171–189.

Wyllie, P. J., 1982. Subduction products to experimental prediction, *Bull. geol. Soc. Am.*, **93,** 468–476.

Yoder, H. S. & Tilley, C. E., 1962. Origin of basalt magmas: an experimental study of natural and synthetic rock systems, *J. Petrol.*, **3,** 343–532.

Yoshii, T., Tada, T., Okada, H., Asano, S., Muramatu, I., Hashizume, M. & Moriya, T., 1974. The third Kurayoshi explosion and the crustal structure in the western part of Japan, *J. Phys. Earth*, **22,** 109–121.